DOKUZ EYLÜL UNIVERSITY
GRADUATE SCHOOL OF NATURAL AND APPLIED SCIENCES

A NOVEL MICROSCOPIC MODELLING OF DISORDER EFFECTS WITHIN THE NON LINEAR SCREENING THEORY IN THE QUANTIZED HALL REGIME

by

Sinem ERDEN GÜLEBAĞLAN

February, 2012
İZMİR

A NOVEL MICROSCOPIC MODELLING OF DISORDER EFFECTS WITHIN THE NON LINEAR SCREENING THEORY IN THE QUANTIZED HALL REGIME

A Thesis Submitted to the
Graduate School of Natural and Applied Sciences of Dokuz Eylül University
In Partial Fulfillment of the Requirements for the Degree
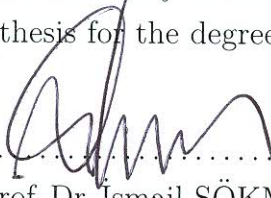of Doctor of Philosophy in
Physics

by
Sinem ERDEN GÜLEBAĞLAN

February, 2012
İZMİR

Ph.D. THESIS EXAMINATION RESULT FORM

We have read the thesis entitled "**A NOVEL MICROSCOPIC MODELLING OF DISORDER EFFECTS WITHIN THE NON LINEAR SCREENING THEORY IN THE QUANTIZED HALL REGIME**" completed by **SİNEM ERDEN GÜLEBAĞLAN** under supervision of **PROF. DR. İSMAİL SÖKMEN** and we certify that in our opinion it is fully adequate, in scope and in quality, as a thesis for the degree of Doctor of Philosophy.

....

Prof. Dr. İsmail SÖKMEN

Supervisor

....
Prof. Dr. Mürüvvet YURDAKOÇ

Thesis Committee Member

....
Assist. Prof. Dr. Kadir AKGÜNGÖR

Thesis Committee Member

....
Prof. Dr. Kemal KOCABAŞ

Examining Committee Member

....
Assoc.Prof.Dr. Afif SIDDIKİ

Examining Committee Member

....
Prof. Dr. Hamza POLAT

Examining Committee Member

....
Assist. Prof. Dr. Uğur ERKASLAN

Examining Committee Member

....

Prof. Dr. Mustafa SABUNCU

Director Graduate School of Natural and Applied Sciences

ACKNOWLEDGEMENTS

It is delight to acknowledge all the people who have supported me over my Ph.D. study.

First of all I wish to express my greatest appreciation and thanks to my supervisor Prof. Dr. İsmail SÖKMEN for his excellent guidance, patience and continual encouragement. Many of the research subjects were initiated by Prof. SÖKMEN and he offered many constructive ideas to solve problems with physics as well as computational fields. Particular thanks go to my second supervisor Assoc. Prof. Dr. Afif SIDDIKİ for his support, contributions especially in preparation of the publications, motivation, fruitful discussions, valuable recommendations. I would like to thank, Prof. Dr. Rolf R. GERHARDTS for all his advice, positive criticism of my thesis. Special thanks go to Assis. Prof. Dr. Kadir AKGÜNGÖR for his advice and support.

I am very grateful to all my friends for the support and their good humor. I would like to thank my husband and my family whom without their continuous support, motivation and encouragement, I would not to be able to complete this work.

Sinem ERDEN GÜLEBAĞLAN

Anneme ve Oğluma ...

A NOVEL MICROSCOPIC MODELLING OF DISORDER EFFECTS WITHIN THE NON LINEAR SCREENING THEORY IN THE QUANTIZED HALL REGIME

ABSTRACT

In this thesis, we studied the effects of disorder on the integer quantized Hall effect within the screening theory, systematically. The disorder potential is analyzed considering the range of the potential fluctuations. Short range part of the single impurity potential is used to define the conductivity tensor elements within the self-consistent Born approximation, whereas the long range part is treated self-consistently at the Hartree level. Briefly, we discussed the extend of the quantized widths Hall plateaus considering the *mobility* of the wafer and the width of the sample, by re-formulating the Ohms law at low temperatures and high magnetic fields.

In the second part of the thesis, discusses a systematic explanation to the unusual non-monotonic behavior of the Hall resistance observed in two-dimensional electron systems. In the calculations used a semi analytical model based on the interaction theory of the integer quantized Hall effect to investigate the existence of the anomalous, i.e. overshoot, Hall resistance. The observation of the overshoot resistance at low magnetic-field edge of the plateaus is elucidated by means of overlapping evanescent incompressible strips, formed due to strong magnetic fields and interactions. The effects of the sample width, depletion length, disorder strength and magnetic field on the overshoot peaks are investigated in detail.

Keywords: Quantum Hall effect, Disorder, Thomas-Fermi Approximation.

QUANTİZE HALL BÖLGESİNDE DOĞRUSAL OLMAYAN PERDELEME TEORİSİ İLE YAPI BOZUKLUKLARININ MİKROSKOBİK MODELLENMESİ

ÖZ

Bu tezde, tamsayılı kuantum Hall sistemlerinde perdeleme kuramı ile safsızlıkların etkisi sistematik olarak incelendi. Safsızlık potansiyeli potansiyel dalgalanmaların erimi analiz edildi. Safsızlık potansiyeli kısa erimli kısmı öz-uyumlu Born yaklaşım ile iletkenlik tensörünü tanımlamak için kullanıldı. Uzun erimli kısmı göz önünde bulundurularak Hartree düzeyde öz-uyumlu olarak ele alındı. Kısaca, düşük sıcaklıklarda ve yüksek manyetik alanlar Ohm kanunu yeniden formüle edilerek, örneğin mobilitesi (hareketliliği) ve genişliği dikkate alınarak Kuantum Hall platosu tartışıldı.

Tezin ikinci kısmında, iki boyutlu elektron sisteminde görülen alışılmamış monotonik olmayan Hall direncindeki değişimi sistematik olarak tartışıldı. Hesaplamalarda, Hall direncindeki bu anormal davranışı araştırmak için tamsayı Kuantum Hall etkisinde etkileşim teorisi üzerine dayalı bir yarı analitik model kullandı. Platoların kenarında düşük manyetik alanlarda görülen overshoot direnci, kuvvetli manyetik alanlarda oluşan sıkıştırılamaz şeritin kalıntılarının üst üste gelmesiyle açıklandı. Overshoot, elektronsuz bölgenin uzunluğuna, örnek boyuna, safsızlıkların büyüklüğüne ve manyetik alana bağlılığı detaylı olarak araştırıldı.

Anahtar sözcükler: Kuantum Hall Olayı, safsızlık, Thomas-Fermi Yaklaşımı.

CONTENTS

CHAPTER ONE
INTRODUCTION

In the past 40 years, semiconductor physics brought a revolution, both in science and in everyday life. The advent of semiconducting devices and their use in integrated circuits was a of a social revolution and clearly marked the brink of a new era. Transistors and diodes became indispensable as they made their way in to pretty much all of every day life. The two-dimensional electron system (2DES) has proven to be a remarkable system for studying fundamental physics at the second half of the 20th century. The 2DES is the subject of the quantum Hall effect.

The quantum Hall effect (QHE) is a transport phenomena occurring in a two dimensional electron or hole system (2DES or 2DHS) under a high magnetic field. The value of the Hall resistance plateau in the *integer quantum Hall effect* (IQHE) is $h/e^2 i$ with $i = 1, 2, ...$ It was firstly discovered by Klaus von Klitzing in 1980, who was honored by the Nobel prize in 1985.

The IQHE was soon followed by another unexpected, even more surprising finding. When carrying out Hall measurements on even cleaner samples, higher fields, and lower temperatures, Tsui, Störmer and Gossard (Tsui et al., 1982) discovered in 1982 that the Hall conductivity becomes quantized also at high magnetic fields or voltages and acquires certain fractional value of e^2/h, such as 1/3, 2/3, 2/5 and so on. Owing to the logic, this effect was called *fractional quantum Hall effect* (FQHE) and rewarded with a Nobel prize in 1998.

In this thesis, we investigated a self-contained calculation scheme to explain the effect of disorder within the interaction theory of integer quantized Hall effect, the observed resistance overshoot and local density of states under strong in-plane electric and perpendicular magnetic fields. The thesis is structured as follows: In chapter 2, we introduce the essential ingredients of the quantum Hall effect. In chapter 3, we have shown the calculations of the disorder effect in a two-dimensional electron sys-

tem. We have investigated evanescent incompressible strips as origin of the observed Hall resistance overshoot. The self consistent calculation to investigate overshooting has been done within Thomas-fermi approximation (TFA), in chapter 4. Finally, the conclusions of the complete thesis are presented in chapter 5.

THE QUANTUM HALL EFFECT

2.1   The Classical Hall Effect

In 1879 Edwin Hall discovered that the application of a magnetic field B perpendicular to a thin conducting slab through which a current flows produces a voltage across the slab and perpendicular to the current (Fig. 2.1). This voltage is called the Hall voltage V_H and the effect itself is called the Hall effect.   So basically the Hall
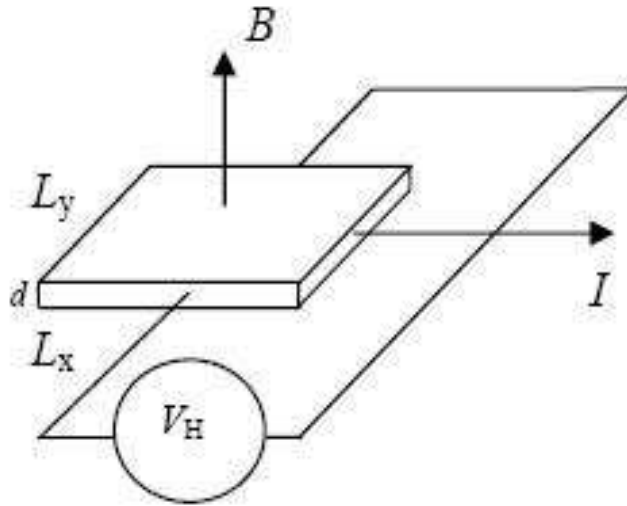
Figure 2.1   Schematic representation of the classical Hall effect.

voltage is caused by the Lorentz force acting on the charges moving in the presence of a magnetic field. In equilibrium the Lorentz force $|F_L| = qv_D B$ is balanced by the electric force qV_H/L_y, where q is the carrier charge, v_D is the drift velocity and L_y is the width of the sample. So $V_H = v_D B L_y$ exhibits a linear dependence on the magnetic field B. Writing the current I as the product of the drift velocity v_D, the charge density n_q and the cross-sectional area of the sample $S = L_y d$, we find the perpendicular resistivity $R_H = V_H/I$ to be

$$R_H = \frac{B}{qn_e d} = \frac{B}{qN_s}, \qquad (2.1.1)$$

where $n_e = n_q/q$ is the number of carriers per unit volume and N_S is the number of carriers per unit surface area. Because the Hall resistance R_H only depends on the magnetic field B and the carrier density and not on other material parameters, the Hall effect has become a standard tool of material characterization. The direct proportionality of the Hall resistivity on the local magnetic field has allowed the development of scanning Hall probe microscopes which allow for instance a detailed determination of the magnetic field distribution near the vortices in type II superconductors. The ordinary Hall effect can be fully explained by classical concepts, considering electron transport in metals, like the Drude model. The fact that there is a quantum mechanical follow-up in the form of the quantum Hall effect which adds totally new dimensions to the study of low dimensional electronic systems, originally came as a complete surprise in physics as a whole (Galistu, 2010).

2.2   The Integer Quantum Hall Effect

The discovery of the ordinary Hall effect and advent of the quantum Hall effect (K. von Klitzing, 1980) are one century apart. The quantum Hall effect has already led to three Nobel prizes in physics, one for the integral quantum Hall effect in 1985 and one for the fractional quantum Hall effect (Tsui , 1999; Laughlin, 1999) in 1998 and in 2010. These robust quantum phenomena on a macroscopic scale, Hall effect manifest themselves in the transport parameters of the two dimensional electron gas that are directly measurable, notably the longitudinal resistance (usually denoted by R_{xx} or R_L) and the Hall resistance (usually denoted by R_{xy} or R_H). Still to date, more than 30 years after the first discovery, our microscopic understanding of the quantum Hall effect is far from being complete. The quantum Hall effect is standard observed in strong perpendicular magnetic fields B and at low temperatures ($T = 4K$) and it is

well known that the phenomenon only exists because of the breaking of translational invariance by random impurities. Instead of the linear dependence of R_H with varying magnetic field B, it now turns out that the Hall resistance is quantized in units of h/e^2

$$R_H = \frac{h}{ie^2} \approx \frac{25812.8}{i}k\Omega \qquad (2.2.1)$$

Here, i is an integer, h denotes Plancks constant and e is the charge of the electron. It is now generally accepted that the transitions between adjacent quantum Hall plateaus are continuous quantum phase transitions that are characterized by a diverging length scale usually termed the localization length of the electrons near the Fermi energy. The longitudinal resistance R_L shows a peak at the transitions but it vanishes at the plateau values of R_H (Galistu, 2010). The quantization phenomenon is extraordinarily accurate. This precision led the International Committee for Weights and Measures (CIPM) to adopt the quantum Hall effect as the new standard for electrical resistance in 1988.

2.3 Two Dimensional Electron Gas in AlGaAs/GaAs Heterostructure

In the quantum Hall effect community, the two dimensional electron gas (2DEG) is usually obtained at $Al_xGa_{1-x}As/GaAs$ heterostructures. Such III-V group materials are preferred to the silicon MOSFET due to its higher electron mobility. A typical layer sequence to create 2DES based on GaAs/AlGaAs is shown in Fig. 2.3a. By using molecular beam epitaxy (MBE), the sharp interface between the AlGaAs and GaAs is realized with perfect crystal quality. Due to a conduction band offset between AlGaAs and GaAs, the AlGaAs layer doped with silicon atoms gives electrons to the GaAs layer. These electrons are trapped at the heterojunction since Si^+ ions create an attractive triangular shaped confinement potential (Fig. 2.3b-c). The electrons in this potential well can freely move in the plane parallel to the interface (x and y di-
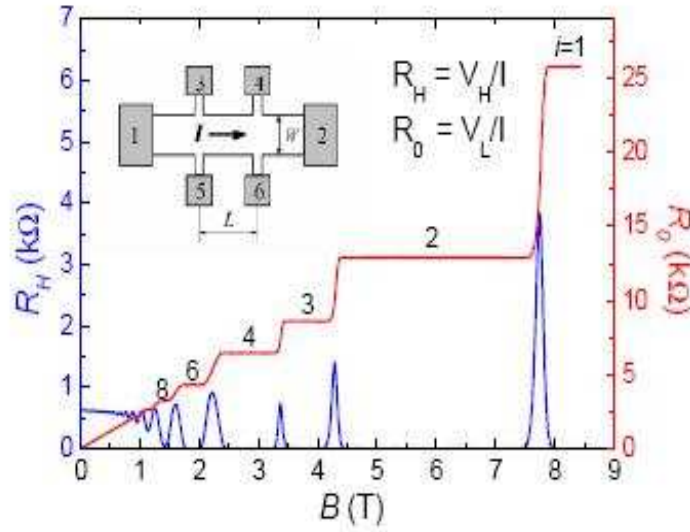
Figure 2.2   Quantum Hall effect measured on a sample with Hall bar geometry (top left corner). The Hall voltage V_H is measured between contacts 3 and 5 or 4 and 6. The longitudinal voltage V_L is measured between contacts 3 and 4 or 5 and 6. Data taken on an InGaAs/GaAs quantum well with electron density $n_e = 2.710^{15} \ m^{-2}$ at $T = 0.03K$).

rections). Their eigenfunctions are plane waves with a wave vector k. In z direction a quantization of the energy occurs due to the spatial confinement. The energy spectrum in k-space is therefore described by

$$\varepsilon_{i,k_x,k_y} = \varepsilon_i^z + \frac{\hbar^2 k_x^2}{2m*} + \frac{\hbar^2 k_y^2}{2m*}, \tag{2.3.1}$$

where $\mu* \approx 0.067 m_0$ is the effective electron mass in GaAs. The integer number $i = 1, 2, 3, ..$ labels the eigenenergy values in z direction. These quantized levels define the subband minimum. At low temperature and for low electron density, all electrons occupy the first subband a two-dimensional electrons system is formed (see Fig. 2.3c). One specificity of 2DES, is its density of states at zero magnetic field which is constant
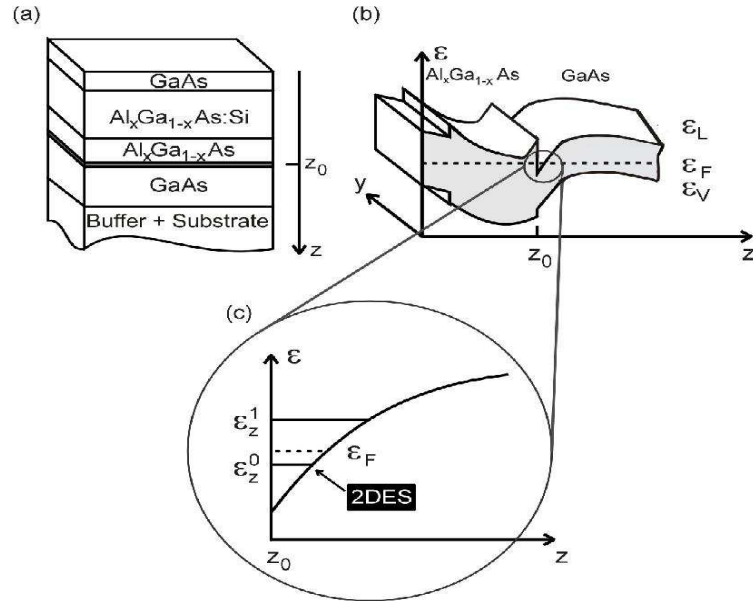
Figure 2.3 Layer sequence of an GaAs/AlGaAs heterostructure. b) Bending of the conduction band minimum and valence band maximum at the junction between the AlGaAs layer and the GaAs layer. A triangle-shaped potential well is formed. c) At respectively low electron density, the electrons at the interface create a 2DES. (Ahlswede, 2002a)

and equal to

$$D(\varepsilon) = D_0 = \frac{m*}{\pi \hbar^2}. \tag{2.3.2}$$

It follows that the Fermi energy, given by

$$\varepsilon_F = \frac{\pi \hbar^2}{m*} n_s, \tag{2.3.3}$$

linearly depends on the sheet electron density n_s (Dahlem, 2008).

2.4 Density of States for Zero Magnetic Field

A two dimensional electron system can be described as a Fermi gas. In such a picture, the interaction between electrons is neglected. It can be assumed that the electron mass is an anisotropic effective mass. This electron is free to move along the x and y directions and a confining potential $V(z)$ along the z direction. We deal with no disorder system. A system is described by the Schöedinger equation and equal to

$$[-\frac{\hbar^2}{2m^*}\nabla^2 + V(z)]\psi(x,y,z) = E\psi(x,y,z) \tag{2.4.1}$$

where $\hbar$ is the Planck constant, E is the energy and $\psi(x,y,z)$ is the wave function. As there is no potential along x and y, the motion of the electron along these directions can be described by plane waves. The solutions of the one-dimensional Schröedinger equation:

$$[-\frac{\hbar^2}{2m^*}\frac{d^2}{dz^2} + V(z)]u_n = \varepsilon_m u_m(z) \tag{2.4.2}$$

where $n = 0, 1, 2, ...$ is a positive integer and $u_n(z)$ are the wave functions corresponding to each quantum number n. If $V(z)$ is an infinite square quantum well:

$$V(z) = \{\infty\ for|z| \geq w/2, 0\ for|z| < w/2\} \tag{2.4.3}$$

where w is the width of the quantum well, then ε_n written as

$$\varepsilon_n = \frac{\hbar^2\pi^2(n+1)^2}{2m^*w^2}, \tag{2.4.4}$$

The total energy of the electron in the 2D system given by

$$E_n(k) = \frac{\hbar^2 k_x^2}{2m^*} + \frac{\hbar^2 k_y^2}{2m^*} + \varepsilon_n \tag{2.4.5}$$

where k is the total wave vector, k_x is the wave vector along the x direction and and k_y is the wave vector y direction. The quantized energy levels along the z direction are well resolved and they are referred as electrical subbands. Once we know the allowed energy levels in the $2D$ system, we can see how its possible to fill them with electrons. We consider a system with a known density of electron n_{2D}. The electron density is given as

$$n_{2D} = \int_{-\infty}^{\infty} D(E)f(E, E_F)dE \tag{2.4.6}$$

where $D(E)$ is the $2D$ density of states (DOS), $f(E, E_F)$ is the Fermi Dirac occupation
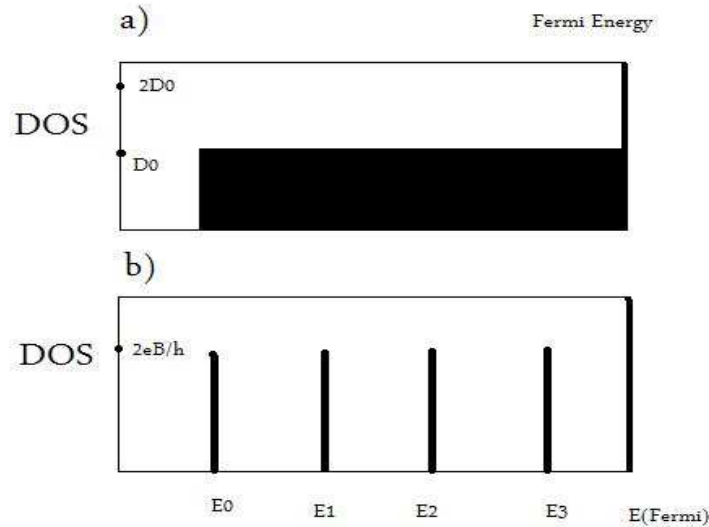
Figure 2.4   Density of states of a 2DES for (a) $B = 0$, (b) $B \neq 0$(no spin).

function and E_F is the Fermi energy. In $2D$ systems, the density of states (DOS) can be decomposed into contributions from each subband. The DOS per unit area for each electrical subbands has a constant value, and reads as

$$D_0 = \frac{m^*}{\pi\hbar^2} \tag{2.4.7}$$

The total DOS then is given by

$$D(E) = D_0 \sum_n \vartheta(E - \varepsilon_n) \tag{2.4.8}$$

where $\vartheta(x)$ is step function. The total DOS is represented in Fig. 2.4(a) and is a step-like function with jumps of D_0 occurring when the energy reach the bottom of an electrical subband ε_n.

2.5 Density of States for a Perpendicular Magnetic Field

If a perpendicular magnetic field B is applied the $2D$ systems, then the Schröedinger equation writes as

$$[\frac{1}{2m^*}(p + eA)^2 + V(z)]\psi(x,y,z) = E\psi(x,y,z) \tag{2.5.1}$$

where p is the canonical momentum operator and A is the magnetic vector potential. This magnetic vector potential can be chosen as $A = (0, Bx, 0)$. The Schröedinger equation can be reformulated

$$[-\frac{\hbar^2}{2m^*}\nabla^2 - \frac{ie\hbar Bx}{m^*}\frac{\partial}{\partial y} + \frac{(eBx)^2}{2m^*} + V(z)]\psi(x,y,z) = E\psi(x,y,z). \tag{2.5.2}$$

One can see from this equation that B only couples to the motion of the electrons

in the plane of the $2D$ system. Through the Lorentz force, the magnetic field drives the electrons in a circular motion at a frequency ω_c, known as cyclotron frequency and written as

$$\omega_c = \frac{|e|B}{m^*} \tag{2.5.3}$$

and with a cyclotron radius r_c of

$$r_c = \sqrt{\frac{\hbar}{eB}} \tag{2.5.4}$$

where e is the electron charge. As the magnetic field only affects the motion of electron within the plane of the $2D$ system and confining potential along the z direction has only an additive contribution, the in-plane and transverse part can be solved separately. The total energy for the electrons

$$E_{n,r} = \varepsilon_n + \hbar\omega_c(r + 1/2) \tag{2.5.5}$$

where n, $r = 0, 1, 2, ...$ are positive integers and ε_n are the transverse electrical sub-bands given by Eq. (2.4.4). The electron energies obtained here and this energies are independent of k. The electrons condensate into highly degenerate energy levels, called Landau levels (LLs). For levels originating in the same transverse electrical subband, the energy gap between two Landau level is $\hbar\omega_c$ while the degeneracy of each level is $2(eB/h)$. The DOS of a 2DES subject to a magnetic field is then given by

$$D(E,B) = 2\frac{eB}{h}\sum_{n,r}\delta(E - E_{n,r}) \tag{2.5.6}$$

where $\delta(x)$ is the delta function. This DOS, represented in Fig. 2.4(b), is made of a series of δ-like LLs. When B is swept up, the LLs move away from each other and are

depopulated when passing through E_F . The increase of B also induces a variation of E_F. Indeed, E_F moves with the DOS in order to keep the number of electrons constant. The evolution of E_F as a function of B is shown in Fig. 2.4 for a perfect 2D systems with δ-like LLs.

2.6 Electric-field-broadened Landau Levels

We describe a 2DES in the *x-y*-plane, subjected to a strong magnetic field $\mathbf{B} = (0,0,B) = \nabla \times \mathbf{A}(\mathbf{r})$ in *z*-direction, in an effective-field (e.g. Hartree) approximation by a single-particle Hamiltonian

$$H = \frac{1}{2m^*}\left(\mathbf{p} + \frac{e}{c}\mathbf{A}(\mathbf{r})\right)^2 + V(\mathbf{r}), \qquad (2.6.1)$$

where the potential energy $V(\mathbf{r})$ may contain the effect of externally applied static electric fields, of lateral confinement, and of the average Coulomb interaction with the other electrons of the 2DES. Once the eigen-functions $\psi_\alpha(\mathbf{r})$ of the Schrödinger equation

$$(H - E_\alpha)\psi_\alpha(\mathbf{r}) = 0 \qquad (2.6.2)$$

are known, one can calculate the electron density

$$n(\mathbf{r}) = \sum_\alpha f_\alpha |\psi_\alpha(\mathbf{r})|^2, \qquad (2.6.3)$$

where the occupation probability f_α of the energy eigenstate $|\alpha\rangle$ may depend on all the quantum numbers of conserved quantities collected in α, i.e., two for orbital motion and one for spin.

2.6.1 Local Density of States (LDOS)

If in Eq. (2.6.3) the occupation probability of the state $|\alpha\rangle$ depends only on its energy eigenvalue, $f_\alpha = f(E_\alpha)$, it may be useful to express the density

$$n(\mathbf{r}) = \int dE\, f(E) D(E;\mathbf{r}) \tag{2.6.4}$$

in terms of the "local density of states" (LDOS):

$$D(E;\mathbf{r}) = \sum_\alpha \delta(E - E_\alpha) |\psi_\alpha(\mathbf{r})|^2. \tag{2.6.5}$$

This formula for the LDOS is easily generalized to include the effect of quasi-elastic scattering of the electrons by randomly distributed impurities, which leads to a "collision broadening" of the δ-function in Eq. (2.6.5).

2.6.2 Translation Symmetry in y-direction

We assume that the system is translation-invariant in y-direction, but electric fields in x-direction, $\mathbf{E} = (E_x, 0, 0) = \nabla V(x)/e$, will be allowed. The translation invariance in y-direction suggests the Landau gauge $\mathbf{A}(\mathbf{r}) = (0, xB, 0)$ for the vector potential, so that the single-electron Hamiltonian (2.6.1) becomes cyclic in y and allows the separation ansatz

$$\psi(x, y) = \frac{e^{iky}}{\sqrt{L_y}} \varphi_k(x), \tag{2.6.6}$$

where L_y ($\to \infty$) is the normalization length in y direction, and the quasi-continuous momentum quantum number k assumes the values $k = 2\pi n_y/L_y$, for arbitrary integers n_y. With this ansatz the Schrödinger equation (2.6.2) reduces to the one-dimensional form

$$H_X \varphi_{n,X}(x) = E_n(X) \varphi_{n,X}(x), \tag{2.6.7}$$

with the effective Hamiltonian

$$H_X = -\frac{\hbar^2}{2m^*}\frac{d^2}{dx^2} + \frac{m^*}{2}\omega_c^2(x-X)^2 + V(x), \qquad (2.6.8)$$

where $X = -\ell^2 k$ denotes the center of the parabolic potential, which describes the effect of the magnetic field and leads for fixed X to a discrete energy spectrum $E_n(X)$. Here and in the following we neglect spin splitting and consider spin by a degeneracy factor $g_s = 2$. In general the eigenstates $\langle \mathbf{r}|n,X\rangle$ carry current in y-direction, and the expectation value of the velocity operator $\hat{v}_y$ is given by (Hellmann-Feynman theorem)

$$\langle n,X|\hat{v}_y|n,X\rangle = -\frac{1}{m^*\omega_c}\frac{dE_n(X)}{dX} \quad \left[\equiv \frac{1}{\hbar}\frac{dE_n}{dk}\right]. \qquad (2.6.9)$$

Then the electron density, Eq. (2.6.3), depends only on x,

$$n(x) = \frac{g_s}{2\pi\ell^2}\sum_n \int dX\, f_{n,X}\,|\varphi_{n,X}(x)|^2, \qquad (2.6.10)$$

and is accompanied by a current density

$$j_y(x) = \frac{g_s e}{2\pi\hbar}\sum_n \int dX\, f_{n,X}\,\frac{dE_n(X)}{dX}|\varphi_{n,X}(x)|^2. \qquad (2.6.11)$$

The LDOS, Eq. (2.6.5), reduces to

$$D(E;x) = \frac{g_s}{2\pi\ell^2}\sum_n \int dX\,\delta(E-E_n(X))\,|\varphi_{n,X}(x)|^2. \qquad (2.6.12)$$

If the dependence of $E_n(X)$ on X is smooth enough to allow for a Taylor expansion around the center coordinate $X_{n,E}$ defined by $E_n(X_{n,E}) = E$, the X-integral in Eq. (2.6.12) can be evaluated:

$$D(E;x) = \frac{g_s}{2\pi\ell^2}\sum_n \frac{|\varphi_{n,X_{n,E}}(x)|^2}{|E_n'(X_{n,E})|} \qquad (2.6.13)$$

with $E'_n(X_{n,E}) = dE_n/dX(X_{n,E})$. Before we illustrate some properties of this LDOS with typical examples, we introduce a simple treatment of collision broadening.

2.6.3 Collision Broadening

2.6.3.1 Homogeneous 2DES without Electric Field

For $V(x) \equiv 0$ we get the well known Landau problem with energy eigenvalues and eigenfunctions

$$E_n = \hbar\omega_c(n+\frac{1}{2}), \quad \varphi_{n,X}(x) = \frac{1}{\sqrt{\ell}} u_n\left(\frac{x-X}{\ell}\right), \qquad (2.6.14)$$

respectively, where the normalized oscillator wavefunctions,

$$u_n(\zeta) = \left(\frac{1}{2^n n! \sqrt{\pi}}\right)^{1/2} H_n(\zeta)\, e^{-\zeta^2/2}, \qquad (2.6.15)$$

are given by the Hermite polynomials $H_n(\zeta)$ of order n (Abramowitz, 1964). Since here the energy eigenvalues are independent of X, the X-integral in Eq. (2.6.12) reduces to the normalization integral of the eigenfunctions, and the LDOS reduces to the well known Landau DOS of the homogeneous system

$$D(E;x) = \frac{g_s}{2\pi\ell^2} \sum_n \delta(E - E_n), \qquad (2.6.16)$$

which does not depend on the position x. To include the effect of collision broadening, one has to evaluate the self-energy operator. With weak assumptions (like rotation symmetry) on the impurity potentials, one can show that $\Sigma(z)$ and the Green operator $G(z)$ are diagonal in the Landau representation, and that the matrix elements together with the eigen-energies $E_n(X)$ do not depend on X (Scher, 1966; Keiter, 1967; Bangert, 1968; Gerhardts, 1975-1). Then in Eq. (2.6.16) the singular $\delta(E - E_n)$ is replaced by a spectral function $A_n(E - E_n)$ of finite width. Depending on the approxi-

mation scheme, several analytical forms for the spectral function have been obtained. The self-consistent Born approximation (SCBA) (Gerhardts, 1975-1; Ando, 1982) leads, if scattering between different Landau levels is neglegted, to a semi-elliptical form,

$$A_n^{\mathrm{SCBA}}(E - E_n) = \frac{1}{\pi \Gamma_n} \left(1 - \left[\frac{E - E_n}{2\Gamma_n} \right]^2 \right)^{\frac{1}{2}}, \qquad (2.6.17)$$

while other approaches yield a Gaussian form, (Gerhardts, 1975-2)

$$A_n^G(E - E_n) = \frac{1}{\sqrt{2\pi}\,\Gamma_n} \exp\left(-\frac{1}{2} \left[\frac{E - E_n}{\Gamma_n} \right]^2 \right). \qquad (2.6.18)$$

In the limit of short-range impurity potentials the matrix elements of the self-energy and thereby the Γ_n in Eqs. (2.6.17) and (2.6.18) become even independent of the Landau quantum number n.

2.7   Exactly Solvable Models

2.7.1   *Constant Electric Field*

Simple analytic results are also obtained for the case of a constant in-plane electric field $\mathbf{E} = (E_x, 0, 0)$, leading to the potential $V(x) = exE_x$. Within classical mechanics, this leads for an ideal 2DES to a constant Hall drift of the centers of the cyclotron motion, which can be eliminated by a Galilei transformation to a coordinate system moving with the drift velocity $\mathbf{v}_D = c\mathbf{E} \times \mathbf{B}/B^2 = (0, -cE_x/B, 0)$. Since all electrons suffer the same drift velocity, the current density $\mathbf{j}(x) = -e\mathbf{v}_D n(x)$ is proportional to the electron density $n(x)$, and one obtains Ohm's law $\mathbf{j}(x) = \hat{\sigma}(x)\mathbf{E}$ with the Hall conductivity $\sigma_{yx}(x) = (ec/B)n(x)$ and vanishing longitudinal conductivity, $\sigma_{xx}(x) \equiv 0$.

2.7.1.1 Eigenstates and LDOS

Inserting $V(x) = exE_x$ into the Hamiltonian (2.6.8) results in a shifted parabolic potential with the new center $\tilde{X} = X - eE_x/(m^*\omega_c^2)$ and position-independent terms, which add to the oscillator energies $\varepsilon_n = \hbar\omega_c(n + 1/2)$. The resulting energy eigenvalues and eigenfunctions are

$$\tilde{E}_n(\tilde{X}) = \varepsilon_n + eE_x\tilde{X} + \frac{m^*}{2}v_D^2 = \varepsilon_n + eE_xX - \frac{m^*}{2}v_D^2 \equiv E_n(X), \qquad (2.7.1)$$

and

$$\varphi_{n,X}(x) = \frac{1}{\sqrt{\ell}}u_n\left(\frac{x - \tilde{X}}{\ell}\right), \qquad (2.7.2)$$

respectively, with $v_D = cE_x/B$. From Eq. (2.6.9) we see that each state carries the same current $-e\langle n, X|\hat{v}_y|n, X\rangle = e^2E_x/m^*\omega_c = ev_D$, in analogy to the fact, that the radius of the classical cyclotron orbit has no influence on the drift velocity of its center. As a consequence of Eqs. (2.6.10) and (2.6.11) the current density is directly proportional to the electron density,

$$j_y(x) = ev_Dn(x), \qquad (2.7.3)$$

independent of the occupation probability of the eigenstates, just as in the classical case.

Due to the linear dependence of $\tilde{E}_n(\tilde{X})$ on $\tilde{X}$, Eq. (2.6.13) can be written as

$$D(E;x) = \frac{g_s}{2\pi\ell^2}\sum_n\frac{1}{e|E_x|\ell}u_n^2\left(\frac{\tilde{E}_n(x) - E}{eE_x\ell}\right). \qquad (2.7.4)$$

This result has been obtained in Ref. (Kramer, 2004) in a much less transparent way, starting from the symmetric instead of the Landau gauge for the vector potential.
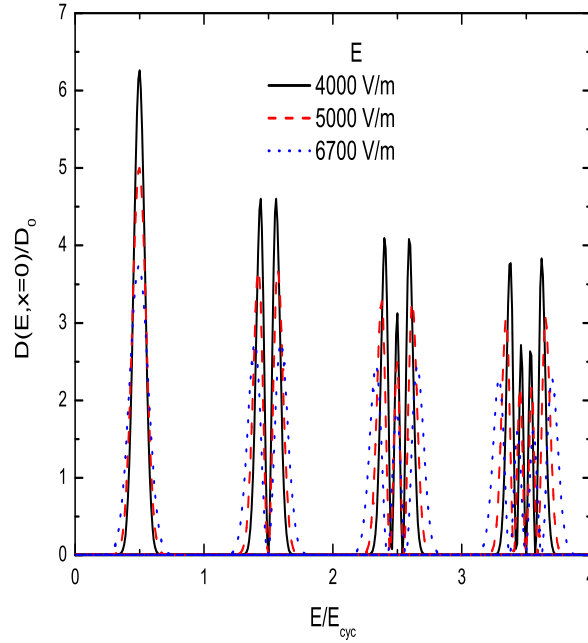
Figure 2.5 Local density of states for different values. $D_0 = m^*/(\pi\hbar^2)$, $g_s = 2$.

The Colored lines in Fig. 2.6 are calculated for a Gaussian spectral function, Eq. (2.6.18), with n-independent $\Gamma_n = \gamma\hbar\omega_c$ for two values of γ. Apparently the zeroes of the LDOS, which are due to the zeroes of the energy eigenfunctions, are smeared out already by a very weak collision broadening, and are of no importance in real samples. A discussion (Kramer, 2004) of a possible importance of these zeroes for the QHE is therefore without any relevance. On the other hand, the value of the LDOS in the gap between two adjacent Landau levels is of importance. In order to yield a plateau in the IQHE, the gap in an incompressible strip between two adjacent compressible regions must be sufficiently well developed. As a measure for the quality of such gaps we may consider the overlap of the contributions of adjacent Landau levels to the LDOS, according to Eq. (2.7.4). We define the overlap as the product of these contributions in the middle $E_{n,n+1}(x) = [\tilde{E}_n(x) + \tilde{E}_{n+1}(x)]/2$ between these levels, devided by the square of the zero-B DOS $D_0 = m^*/(\pi\hbar^2)$, to make the overlap dimensionless. Since
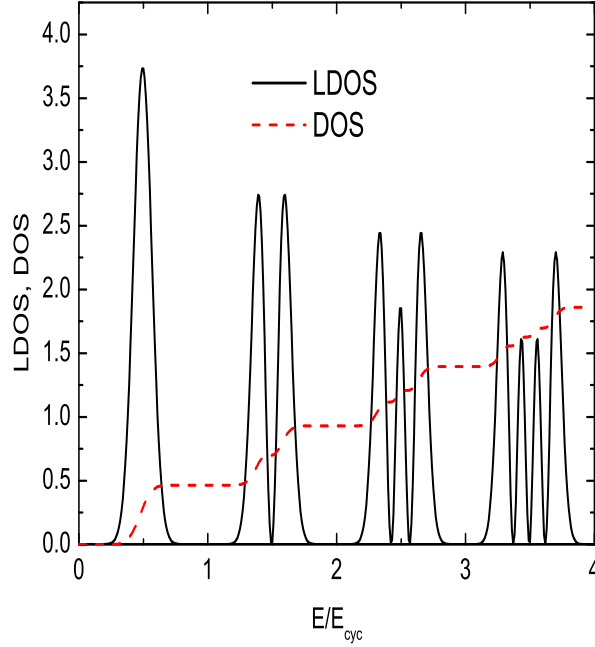
Figure 2.6   Local density of states and density of states for 6700 V/m. $D_0 = m^*/(\pi\hbar^2)$, $g_s = 2$.

$g_s/(2\pi\ell^2 D_0) = \hbar\omega_c$, Eqs. (2.7.1) and (2.7.4) yield for the dimensionless overlap of level n and $n+1$:

$$O_{n,n+1}(\eta) = \frac{1}{\eta^2} u_n^2\left(-\frac{1}{2\eta}\right) u_{n+1}^2\left(\frac{1}{2\eta}\right), \qquad (2.7.5)$$

with $\eta = e|E_x|\ell/\hbar\omega_c$. The results for the lowest gaps, $O_{0,1}(\eta) = \exp(-1/2\eta^2)/(2\pi\eta^4)$ and $O_{1,2}(\eta) = O_{0,1}(\eta)(2 - 1/\eta^2)^2/8$, are plotted in Fig. 2.7.

If we say that the gap between Landau level n and $n+1$ is well developed if $O_{n,n+1} < 10^{-8}$, this defines a critical value $\eta_{n,n+1}^{cr}$ ($\eta_{0,1}^{cr} \approx 0.15$, $\eta_{1,2}^{cr} \approx 0.13$) and thereby a critical field-strength $E_{n,n+1}^{cr} = \eta_{n,n+1}^{cr}\hbar\omega_c/e\ell$. Only for sufficiently small
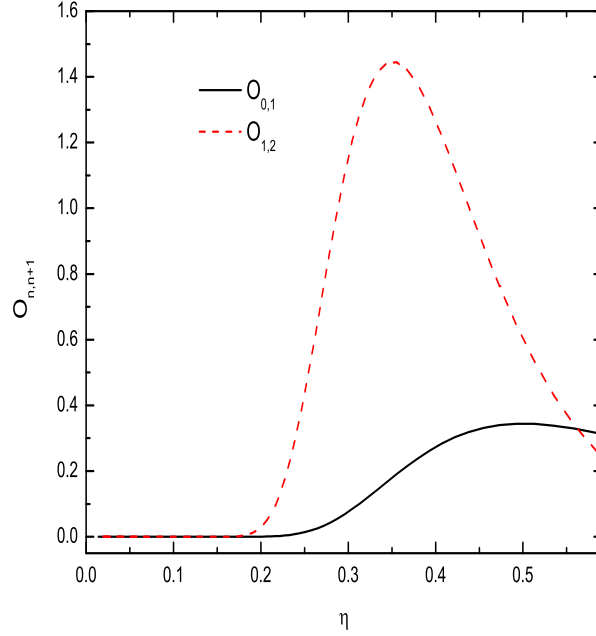
Figure 2.7 a) Two-dimensional local density of states and density of states at electric field ($6700eV$) and a magnetic field ($6\,T$) as a function of the energy. b) Filling factor as a function of the energy.

electric fields with

$$|E_x| \lesssim 2.1 \eta_{n,n+1}^{cr} (B/10\text{T})^{3/2} \times 10^6 \, \text{V/m} \qquad (2.7.6)$$

the gap between the Landau levels n and $n+1$ is well developed.

2.8 The Edge State Model

One of the theoretical models put forward to explain the QHE, the Edge state model, at the edges of a real sample the confining potential produces an upward bend-

ing of the Landau levels. The Fermi energy a one-dimensional edge channel is formed for each Landau level. This situation corresponds to the trajectories of an electron moving along the edge of the device in a magnetic field in the classical. As a result, there exist extended states at the Fermi energy near the sample boundaries. Soon after the discovery of the QHE, Halperin recognized (Halperin, 1982) the importance of these edge channels in the transport properties of the 2DEG. Several edge-related theories were then developed, based on different approaches (Streda, 1983).

However, it was in combination with the Landauer formalism (Landauer, 1957) for transport that the edge state approach proved to be really very efficient to understand electrical transport at high field. In the following, we very briefly summarize the approach adopted by Buttiker (Buettiker, 1988), although some pioneering work was done by Streda et al (Streda, 1983) and by Jain et al (Jain, 1988). For additional information, excellent review paper have been published on the subject (Buettiker, 1986).

In the Landauer formalism of transport, the current is taken as the driving force and the electric field can be obtained by calculating the charge distribution due to the current flow. Using transmission and reflection probabilities, the current is given as a function of the electrochemical potential at the contacts. For a single edge state k located between two electron reservoirs at electrochemical potential μ_1 and μ_2, the current fed by the contact in the absence of scattering is

$$I = ev_d D(E)(\mu_1 - \mu_2) = \frac{e}{h}\Delta\mu, \tag{2.8.1}$$

where v_d is the drift velocity of the electron which is proportional to the slope of the Landau level and therefore has an opposite sign on each side of the device. The density of states $D(E)$ is given by $D(E) = 2\pi\hbar v_d$ in a one-dimensional channel. The voltage drop V between the reservoirs is $eV = \Delta\mu$ and the two-terminal resistance of the edge

state is $R = h/e^2$. For N channels, one obtains

$$R = \frac{h}{e^2}\frac{1}{N}.\qquad(2.8.2)$$

2.9   Compressible and Incompressible Strips in the Depletion Region of a 2DES

The model of edge states is a single electron picture.The Landau levels are moved up in energy by the confining potential in this model. The Landau levels are well divided and the electron density increases from zero at the edge in steps of $n_L = \frac{eB}{h}$. The electron density and the local filling of the Landau levels as a function of distance to the edge are shown in Figs. 2.8a, 2.8b. The electron density are very unphysical as they indicate regions of high electric field which mobile carriers would be expected to screen. Coulomb interactions were considered by Chklovskii (Chklovskii et all, 1982) using self consistent descriptions of the edge potential. They found that the sample is divided into incompressible and compressible strips. In the following we summarize the findings of Ref.(Chklovskii et all, 1982);

At zero field the electron density increases smoothly from zero at the edge to the bulk value n_s and has the form:

$$n(x) = (\frac{x - d_\ell}{x + d_\ell})^{1/2},\qquad(2.9.1)$$

for $x > d_\ell$ where d_ℓ is the depletion length and for an etched structure can be approximated by (Lier, 1994):

$$d_\ell \approx \frac{4V_d\varepsilon\varepsilon_0}{\pi e n_s}\qquad(2.9.2)$$

Here V_g is the band gap potential. Fig. 2.8d is plotted as a dashed line, $n(x)$. In a magnetic field the electron distribution obtained from the electrostatics, but the distribution that is would not be expected to alter significantly. This is because of the huge amount of work that would need to be performed against the electric field. The electron distribution in a magnetic field with a self consistent approach is shown that in Figs. 2.8c and 2.8d. The energy gap between the Landau levels means that the electrostatic solution derived at zero field is no longer the lowest energy state. In regions where there is a transition between filling one Landau level. For example at x_1 in Fig. 2.8c, the energy gap means it is energetically favourable to relocate some electrons from the higher Landau level to the lower one. This relocation of charge forms dipolar stripes at the positions x_d and the Landau level density:

$$x_d = \frac{d_\ell}{1 + (\frac{k}{v})^2}, \qquad (2.9.3)$$

where v is the bulk filling factor and $k = int(v)$ the number of completely filled Landau levels. The potential drop across the dipolar stripes equals the energy gap between the Landau levels $\hbar\omega_c$, the width of the stripes a_k can then be estimated from the zero field density gradient at the points x_d:

$$a_k = \left(\frac{2\kappa\Delta E}{\pi^2 e^2 \frac{dn_{\text{el}}(x)}{dx}|_{x_k}} \right)^{1/2}, \qquad (2.9.4)$$

where κ is the dielectric constant of the material and ΔE is determined by the single particle energy gap. The compressibility κ of an electron gas is defined as:

$$\kappa^{-1} = n_s^2 \frac{\partial \mu}{\partial n}. \qquad (2.9.5)$$

Within the dipolar stripes it costs energy $\hbar\omega_c$ to add an electron, the compressibility is therefore zero and these regions are described as 'incompressible'. In the compressible strip, the electrons can be added with small energies (Suddards, 2007).
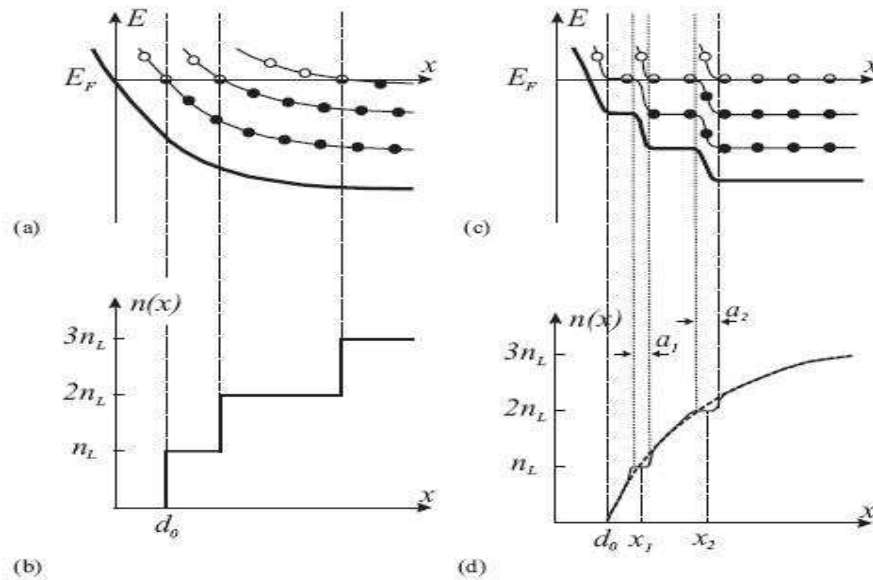
Figure 2.8   Structure of spinless edge states in the integer quantum Hall regime. (a) and (b) single electron picture. (c) and (d) Self-consistent electrostatic picture. (a) Bending of the Landau levels by the confining potential, edge states are then formed at the intersection of the Landau levels with the Fermi energy. (b) Electron density as a function of distance to the boundary, the sudden changes in density would require high electric fields and are unphysical. (c) 2DEG separates into regions of: (i) non-integer filling factor, where Landau levels are pinned at the Fermi energy. Here the 2DEG is compressible and screens the confining potential, and,(ii) regions of integer filling factor where a dipolar stripe has been formed. Here the 2DEG is incompressible and is unable to screen. (d) Density as a function of distance from the boundary. The dashed line shows the density distribution at zero field. At high field this is not significantly modified except in the regions where the next Landau level begins to fill. Based upon Ref. (Chklovskii et all, 1992)

CHAPTER THREE
THE SELF CONSISTENT SCHEME AND THOMAS FERMI APPROXIMATION

3.1 The Self-consistent Scheme

In this section we summarize the numerical calculation algorithm that provides a consistent explanation to the IQHE. We consider a 2DES confined to the interval $-d < x < d$, where d is the half-width of the sample. The repulsive Coulomb interaction among the electrons is described by the Hartree potential,

$$V_{\mathrm{H}}(x) = \frac{2e^2}{\kappa} \int_{-d}^{d} dx' K(x,x') n_{\mathrm{el}}(x'). \tag{3.1.1}$$

Here $K(x,x')$ is the kernel satisfying the boundary conditions, $V(-d) = V(d) = 0$, given as

$$K(x,x') = \ln \left| \frac{\sqrt{(d^2 - x^2)(d^2 - d'^2)} + d^2 - x'x}{(x - x^2)d} \right|. \tag{3.1.2}$$

Then the total potential (energy) of the electron is determined by

$$V(x) = V_{\mathrm{bg}}(x) + V_{\mathrm{H}}(x), \tag{3.1.3}$$

where, the first term is the background potential describing the external electrostatic confinement due to the donors and is given by

$$V_{\mathrm{bg}}(x) = -E_0 \sqrt{1 - (x/d)^2}. \tag{3.1.4}$$

Here $E_0 = 2\pi e^2 n_0 d / \kappa$ is the minimum of the confinement. The solution involves the self-consistent determination of the electron density via

$$n_{\mathrm{el}}(x) = \int dE D(E) f(E + V(x) - \mu^*) \tag{3.1.5}$$

which is valid in the approximation of a slowly-varying potential, the namely Thomas-Fermi approximation (TFA). Here, $f(E) = 1/[\exp(E/k_B T) + 1]$ is the Fermi distribu-

tion function with k_B Boltzmann constant. The density of states $D(E)$ is to be taken from self-consistent Born approximation (Ando, 1982) and μ^* is the constant equilibrium electrochemical potential. Since, the overshoot effect is independent of the actual origin of the single particle gap, from now on we assume spin degeneracy and neglect Zeeman splitting. The density of states (DOS) and local conductivities are determined assuming an impurity potential having a Gaussian form (Ando, 1982)

$$V(r) = \frac{V_I}{\pi R_g^2} \exp(-\frac{r^2}{R^2})$$
(3.1.6)

where the range R_g is of the order of the spacing between 2DES and doping layer, together with the impurity strength V_{imp}. In strong magnetic fields, the Landau levels are broadened due to the scattering from the impurities and the level width is given by

$$\Gamma^2 = 4\pi N_I^2 V_{imp}^2/(2\pi l^2) = (2/\pi)\hbar\omega_c\hbar/\tau,$$
(3.1.7)

where N_I is the number density of the impurities and τ is the momentum relaxation time. We express the widths by the magnetic energy to characterize the impurity strength by the dimensionless ratio $\gamma = \Gamma/\hbar\omega_c$ and define the strength parameter as calculated at 10 T as

$$\gamma_I = [(2N_I V_0^2 m^*/\pi\hbar^2)(1.73 \text{ meV})]^{1/2}.$$
(3.1.8)

The above set of equations allow us to determine the electron density, electrostatic potential and local conductivities in a self-consistent manner when solved numerically by means of successive iterations. The details of the calculation scheme is described in detail elsewhere (Siddiki, 2004).

3.2 Thomas Fermi Approximation

The Thomas-Fermi theory which based on a semi-classical approximation is a local density functional which has been put on a mathematically rigorous basis (Lieb, 1981) and also has been analyzed in 2D in detail by Lieb and group (Lieb, Solovej, 1995). The theory provides a functional form for the kinetic energy of a non-interacting electron gas in some known external potential V (r) as a function of the density and has been successfully applied in the electronic- structure calculations of, e.g., quantum Hall systems, where the importance of e-e interactions has been addressed (Siddiki, 2003; Siddiki, 2007).

CHAPTER FOUR
THE EFFECT OF DISORDER WITHIN THE INTERACTION THEORY OF INTEGER QUANTIZED HALL EFFECT

4.1 Introduction

The integer quantized Hall effect (IQHE), observed at two dimensional charge systems (2DCS) subject to strong perpendicular magnetic fields B. These quantized energy levels are called the Landau levels (LLs). LLs are given by $E_N = \hbar \omega_c (n + 1/2)$, where $\omega_c = eB/m^*c$ is the cyclotron frequency of an electron with an effective mass m^* ($\approx 0.067 m_e$) and n is the Landau index and c is the speed of light in vacuum. Disorder can be created by inhomogeneous distribution of dopant ions. In the absence of disorder, the density of states are $D(E) = \frac{1}{2\pi l^2} \sum_{N=0}^{\infty} \delta(E - E_N)$ (Dirac delta-functions). Here $l = \sqrt{\hbar/eB}$ is the magnetic length, and the longitudinal conductivity (σ_l) vanishes. For a homogeneous two dimensional electron system (2DES), by the inclusion of disorder and due to collisions, LLs become broadened. Therefore the longitudinal conductance becomes non-zero in a finite energy interval. Long range potential fluctuations generated by the disorder result.

We should note that, after decades of study of the influence of disorder on the integer quantum Hall effect, the self-consistent treatment of *electron-electron interactions* and its effect on the disorder potential are not yet investigated from the theoretical point of view, explicitly *at finite* temperatures. At this point, we mention the recent work by A. A. Greshnov and G. G. Zegrya (Greshnov, 2007), where they calculate the maxima of the conductivity peaks and plateau widths depending on the correlation length (λ) of the disorder potential. In this work the conductivities are obtained by assuming a Gaussian random distribution of the impurities and ranges of the single impurities are classified to be short and long range compared to the magnetic length. However, the calculations disregard i) The boundary effects due to confinement ii) Finite size effects, such as actual widths of the samples iii) The electron-electron interactions even at a mean-field level and iv) Temperature effects. This work might be

relevant to localization assumption based explanation of the integer quantized Hall effect, however, the results presented are not clear in physical dimensions (figures have either no scales or are in arbitrary units) and the presented fluctuations of the Hall conductance at the *quantized* Hall regime makes the work highly questionable. Our work takes into account all the points mentioned, meanwhile the Hall plateaus are exactly quantized at vanishing temperature.

The recent experimental (Ruhe, 2006; Mares, 2009; Siddiki et all., 2009) and theoretical (Hwang, 2008; MacLeod, 2009) results point the incomplete treatment of the disorder potential and scattering mechanisms. In particular, the experiments performed at gate defined narrow samples show unexpected asymmetries of the quantized Hall plateaus. To be explicit, one expects that the high temperature Hall resistance should cut through the quantized Hall plateau at the center. This magnetic field value is known as the critical value B_C and important parameters of the scaling theory, *e.g.* localization length, strongly depends on its symmetry around the plateau. However, at the above mentioned experiments (and related theories) it is explicitly shown that the classical line is strongly shifted from the center due to electron-electron interactions and scattering from the edges. Since, none of the previous theories handle the electron-electron interactions self-consistently at finite temperatures such an asymmetry cannot be explained.

In fairly recent theoretical approaches (Guven, 2003) the QH plateaus are obtained by the inclusion of direct Coulomb interaction self-consistently (Siddiki, 2004). In these approaches, the effect of disorder is two-fold: i) The Landau levels are broadened due to collisions and the actual widths of the levels are calculated within the self-consistent Born approximation (SCBA) (Ando, 1982). Such a treatment provides a prescription to calculate longitudinal and transverse conductivities, regardless of the origin of the disorder, i.e. whether they are due to surface roughness, interface roughness or due to Coulomb (donor) impurities. To be explicit, the single impurity potentials are assumed to be Gaussian, randomly distributed all over the sample

and the conductivities are calculated by making spatial averaging over all possible configurations. ii) The overall electrostatic potential landscape fluctuates due to the overlap of many impurities, hence, the inclusion of electron-electron interactions in a self-consistent manner becomes important. In previous works, we explicitly include the effect of level broadening via SCBA and assumed that the potential fluctuations are less pronounced at high mobility samples. Later, this effect is also included in a self-consistent way (Gerhardts, 2008; Siddiki, 2007), however, the investigations of the plateau widths is somewhat non-systematic.

This work provides a systematic investigation of the disorder potential and its influence on the quantized Hall effect including direct Coulomb interaction. The investigation is extended to realistic experimental conditions in determining the widths of the quantized Hall plateaus. We, essentially study the effect of disorder in two distinct regimes, namely the short range and the long range. The short range part is included to the density of states (DOS), thereby influences the widths of the current carrying edge-states and the entries of the conductivity tensor. The long range part is incorporated to the self-consistent calculations. In Sec 4.2 we introduce two types of single impurity potentials, namely the Coulomb and the Gaussian, and compare their range dependencies considering damping of the dielectric material. In the next step we discuss the *screened* disorder potential within a pure electrostatic approach, by considering an homogeneous two dimensional electron system (2DES) without an external magnetic field and show that the long range part is well screened, whereas the short range part is almost unaffected. Section 4.2.3 is devoted to investigate the screening properties of the impurities numerically, where we solve the Poisson equation self-consistently in three dimensions. The numerical and analytical calculations are compared, considering the estimations of the disorder potential range and its variation amplitude. We finalize our discussion with Sec. 4.3, where we calculate the plateau widths under experimental conditions for different sample widths and mobilities.

We would like to note that, the quantized Hall effect and its relation with the disorder effects within the single particle non-interacting models are discussed in many contexts in the last three decades. Therefore it is obviously impossible to mention all the contributions to the field, however, the essentials can be found in many standard text books (Datta, 1995) or well accepted reviews. In contrast, our work takes into account single particle interactions in an explicit and self-consistent manner, whence we obtain the quantized Hall effect even in the (approximately) no-disorder limit.

4.2 Impurity Potential
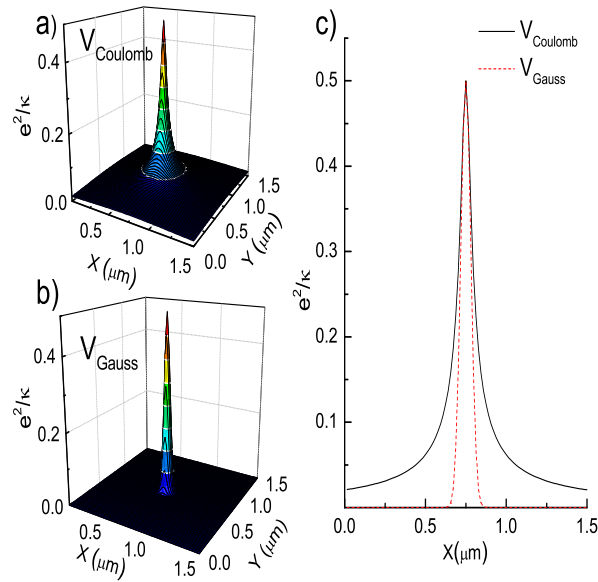
Figure 4.1 (Color online) A single Coulomb (a) and a Gaussian impurity (b) located at the center of a $1.5\mu m \times 1.5\mu m$ unit cell, approximately 30 nm above the electron gas ($z = z_0 = 0$). The short range behaviors are similar, whereas long range parts are strongly different. Potential profiles projected through the center (x, $y = 0.75$ μm), for the Coulomb (solid (black) line) and Gaussian impurity (broken (red) line).
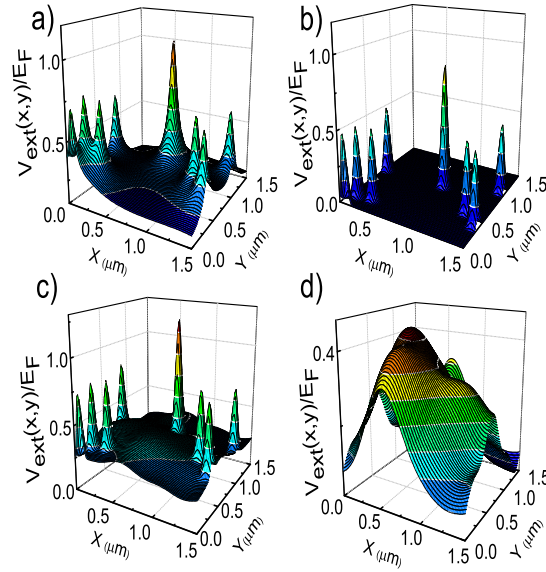
Figure 4.2 External potential generated 30 nm below a plane containing ten (a) Coulomb and (b) Gaussian donors. The range of the Gaussian potential is determined by the spacer thickness. (c) The long range part of the Coulomb potential profile, where only lowest two Fourier components are back-transformed to configuration space. (d) Gaussian potential profile plus the long range part of the Coulomb potential to compare the different potential landscapes.

The disorder potential experienced by the 2DES, resulting from the impurities has quite complicated range dependencies. It is common to theoreticians to calculate the conductivities from single impurity potentials, such as Gaussian (Ando, 1982), Lorentzian (Güven, 2003) or any other analytical functions (Champel, 2008; Kramer, 2006).

In this section we first discuss the different range dependencies of the Coulomb and Gaussian donors located at the center of a unit cell that presumes open boundary conditions. Next, the effect of the spacer thickness on the disorder potential is

shown, namely the damping of the external (Coulomb) potential, and is compared with the Thomas-Fermi screening. The different damping/screening dependencies of the resulting potentials are discussed in terms of range. In the last part we show the distinguishing aspects of the total screened disorder potential such that the long range part is suppressed, however, the short range part is still effective.

4.2.1 Coulomb vs. Gaussian

The electrostatic potential at (x_0, y_0, z_0), created by a single, positively charged particle (ionized donor) placed at x, y, z_D is given by

$$V(x_0, y_0, z_0) = \frac{e^2/\bar{\kappa}}{\sqrt{(x_0-x)^2 + (y_0-y)^2 + (z_0-z_D)^2}} \quad , \qquad (4.2.1)$$

where z_D and z_0 labels the z position of the donor layer and the electron gas, respectively, and $\bar{\kappa}$ is the average dielectric constant (~ 12.4 for GaAs). Throughout this paper we assume that the 2DES resides on $z = z_0 = 0$ plane and the donors are placed at a the finite distance (spacer thickness) $z_D > 0$, hence, the divergencies that may occur at the above equation are ruled out. In principle Eq. 4.2.1 provides a correct description of the impurity potential generated by an ionized donor, however, unfortunately such a description is not useful to define conductivities analytically (Ando, 1982). Instead, one usually considers a Gaussian impurity with an potential amplitude V_{imp} generating a potential at the (x_0, y_0) plane

$$V(x_0, y_0, 0) = -\frac{e^2 V_{\text{imp}}}{\bar{\kappa}|z_D|} \exp\left[-\frac{(x_0-x)^2 + (y_0-y)^2}{2z_D^2}\right]. \qquad (4.2.2)$$

These potentials are shown in Fig. 4.1 for a unit cell of a square lattice with a relevant average dielectric constant $\bar{\kappa}$ considering a single donor residing at the center. Since, the donor is at a finite distance from the plane where the electrostatic potential is calculated, no singularity is observed in the potential distribution. We should note that

the electrostatic potential created by the donor is *damped* (we use the term damped, not to mix with screened) by the dielectric material, which lays between the donor layer and the plane where we calculate the potential. The Coulomb potential presents long range part, which leads to long range fluctuations due to overlapping if several donors are considered within the unit cell, whereas, the Gaussian potential decays exponentially on the length scale comparable with the separation thickness. In Fig. 4.2 we plot the potential generated by 10 donors distributed randomly at the $z = z_D \approx 30$ nm plane, both Coulomb type (Fig. 4.2a) and Gaussian type (Fig. 4.2b), together with the long range part of the Coulomb potential (c). Since the Gaussian potential is relatively short ranged, it is clearly seen that, no overlapping of the single donor potentials occur. Hence, the external potential experienced by the electrons can be approximated to a homogeneous potential fairly good on a length scale $\gtrsim 0.5$ μm. From the above observation one can conclude that approximating the impurity potential by Gaussian potentials is not sufficient to recover the long range part of the disorder potential. Similar arguments is found also in the literature Efros (1988), Siddiki (2007), Nixon (1990). In order to overcome the difference observed at the long range potential fluctuations between the Coulomb and the Gaussian impurities, the following procedure is applied: We perform a two-dimensional Fourier transformation of the Coulomb potential and make a back transformation keeping the first few momentum q components in each direction, hence only the long range part of the potential is left. Then we add the long range part of the Coulomb potential to the potential created by donors, *i.e.* the confinement potential. We take this as a motivation to simulate the short range part of the impurity potential by Gaussian impurities, and calculate the Landau level broadening and the conductivities, described within the self-consistent Born approximation (Ando, 1982) (SCBA). The long range part of the disorder potential is simulated by a (long range) modulation potential and is added to the confining potential, as we describe in sec. 4.3.3.

4.2.2 Pure Electrostatics

We first discuss the different range dependencies of the Coulomb and Gaussian donors, assuming open boundary conditions. Next, the effect of the spacer thickness on the disorder potential is discussed, namely the damping of the external (Coulomb) potential, and is compared with the Thomas-Fermi screening. The different damping/screening dependencies of the resulting potentials are discussed in terms of range.

The Coulomb potential presents long range part, which leads to long range fluctuations due to overlapping if several donors are considered. Whereas, the Gaussian potential decays exponentially on the length scale comparable with the separation thickness. Since the Gaussian potential is relatively short ranged, no overlapping of the single donor potentials occur. Hence, the external potential experienced by the electrons can be approximated to a homogeneous potential fairly good. Thus one can conclude that approximating the total disorder potential by Gaussians is not sufficient to recover the long range part. Similar arguments are also found in the literature (Nixon, 1990; Efros, 1988; Siddiki, 2007). In order to overcome the difference observed at the long range potential fluctuations between the Coulomb and the Gaussian impurities, the following procedure is applied: First we calculate the total disorder potential considering many impurities then we perform a two-dimensional Fourier transformation of the Coulomb potential and make a back transformation keeping the first few momentum q components in each direction, hence only the long range part of the potential is left (Siddiki, 2007). Then we add the long range part of the Coulomb potential to the potential created by donors, *i.e.* to the confinement potential. We take this as a motivation to simulate the short range part of the impurity potential by Gaussian impurities, and calculate the Landau level broadening and the conductivities, described within the self-consistent Born approximation (SCBA) (Ando, 1982). Here we point to the effect of the spacer thickness on the impurity potential experienced in the plane of 2DES. It is well known from experimental and theoretical investigations
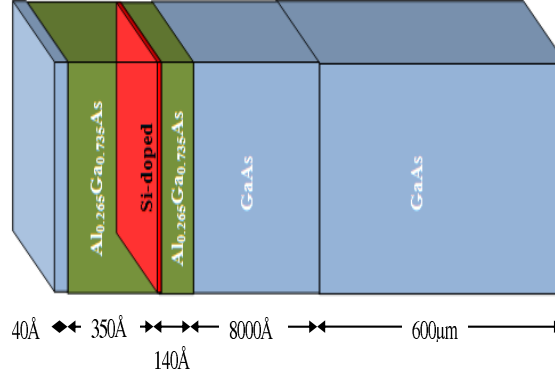
Figure 4.3 Schematic representation of the crystal, which we investigate numerically. The crystal is grown on a thick GaAs substrate, where the 2DES is formed at the interface of the Al-GaAs/GaAs hetero-junction. The top AlGaAs layer is doped with Silicon 30 nm above the interface. The crystal is spanned by a 3D matrix ($128 \times 128 \times 60$).

that, if the distance between the electrons and donors is large, the mobility is relatively high and it is usually related with suppression of the short range fluctuations of the disorder potential. These results agree with the experimental observations of high mobility samples and are easy to understand from the z dependence of the Fourier expansion of the Coulomb potential,

$$V^{\vec{q}}(z) = \int d\vec{r} e^{-i\vec{q}\cdot\vec{r}} \sum_j^N \frac{e^2/\bar{\kappa}}{\sqrt{(\vec{r}-\vec{r}_j)^2 + z^2}} = \frac{2\pi e^2}{\bar{\kappa} q} e^{-|qz|} N S(\vec{q}), \qquad (4.2.3)$$

where $S(\vec{q})$ contains all the information about the in-plane donor distribution and N is the total number of the ionized donors. We observe that if the spacer thickness is increased, the amplitude of the potential decreases rapidly. We also see that the short range potential fluctuations, which correspond to higher order Fourier components, are suppressed more efficiently.

Next, we discuss electronic screening of the external potential created by the donors discussed above. For a dielectric material the relation between the external and the screened potentials are given by,

$$V_{\text{scr}}^q = V_{\text{ext}}^q / \varepsilon(q), \qquad (4.2.4)$$

where $\varepsilon(q)$ is the dielectric *function* and is given by $\varepsilon(q) = 1 + \frac{2\pi e^2 D_0}{\bar{\kappa}|q|}$, with the constant 2D density of states $D_0 = m/(\pi\hbar^2)$ in the absence of an external B field, and is known as the Thomas-Fermi (TF) function. The simple linear relation above, together with the TF dielectric function essentially describes the electronic screening of the Coulomb potential given in Eq. 4.2.3, if there are sufficient number of electrons (Efros, 1988) ($n_{\text{el}} > 0.1 \cdot 10^{15}$ m^{-2}). Consider a case where the q component approaches to zero, then the external (damped) potential is well screened, hence the long range part of the disorder potential. Whereas, the short range part remain unaffected, *i.e.* high q Fourier components. Now we turn our attention to the second type of impurities considered, the Gaussian ones. As well known, the Fourier transform of a Gaussian is also of the form of a Gaussian, therefore, similar arguments also hold for this kind of impurity.

We should emphasize once more the clear distinction between the effect of the spacer on the external potential and the screening by the 2DES, *i.e.* via $\varepsilon(q)$. The former depends on the Fourier transform of the Coulomb potential and the important effect is the different decays of the different Fourier components (see Eq. 4.2.3), so that the short range part of the disorder potential is well dampened, whereas the latter depends on the relevant DOS of the 2DES and the screening is more effective for the long range part.

We continue our investigation by solving the 3D Poisson equation iteratively for randomly distributed single impurities, where three descriptive parameters (*i.e.* the number of impurities, the amplitude of the impurity potential and the separation

thickness) are analyzed separately. Next, we discuss the long range parts of the potential fluctuations investigating the Coulomb interaction of the 2DES, numerically. The range is estimated from these investigations by performing Fourier analysis and is related to the samples used in experiments (Horas, 2008) (Sec. 4.4).
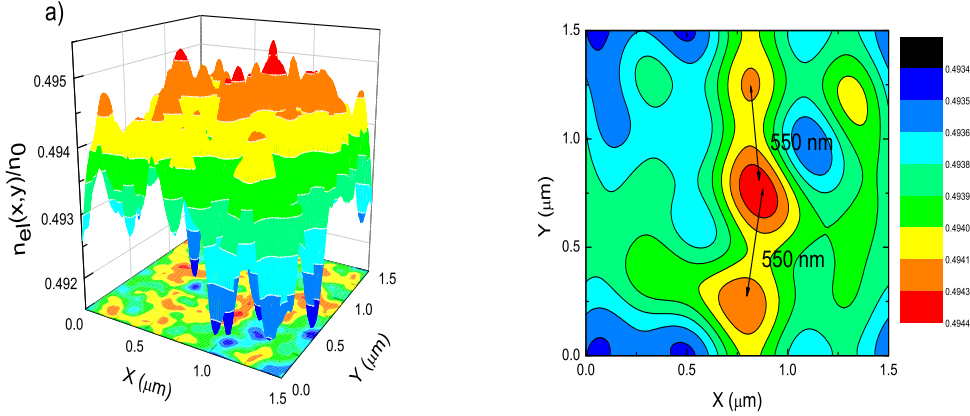

Figure 4.4 (a) Electron density fluctuation considering 3300 impurities 30 nm above the electron gas. (b) The long-range part, arrows are to guide the distance between two maxima. The calculation is repeated for 50 random distributions, which lead to a similar range.

4.2.3 3D Simulations

In the previous section we took a rather simple way to study the effect of interactions by assuming an homogeneous 2DES and screening is handled by the TF dielectric function. Here, we present our results obtained from a rather complicated numerical method. We solve the Poisson equation in 3D starting from the material properties of the wafer at hand, the typical material we consider is sketched in Fig. 4.3. Namely, using the growth parameters, we construct a 3D lattice where the potential and the charge distributions are obtained iteratively assuming open boundary conditions, *i.e.* $V(x \to \pm\infty, y \to \pm\infty, z \to \pm\infty) = 0$. For such boundary conditions, we chose a lattice size which is considerably larger than the region that we are interested in. We preserve the above conditions within a good numerical accuracy (absolute error of 10^{-6}).

A forth order grid approach (Weichselbaum, 2003) is used to reduce the computational time, which is successfully used to describe similar structures (Arslan, 2008).

Figure 4.3 presents the schematic drawing of the hetero-structure which we are interested in. The donor layer is $\delta-$ doped by a density of 3.3×10^{16} m^{-2} (ionized) Silicon atoms, ~ 30 nm above the 2DES, which provide electrons both for the potential well at the interface and the surface. It is worthwhile to note that most of the electrons ($\sim \%90$) escape to the surface to pin the Fermi energy to the mid-gap of the GaAs. In any case, for such wafer parameters there are sufficient number of electrons ($n_{\mathrm{el}} \gtrsim 3.0 \times 10^{15}$ m^{-2}) at the quantum well to form a 2DES. To investigate the effect of impurities we place positively charged ions at the layer where donors reside. From Eq. 4.2.3 we estimate the amplitude of the potential of a single impurity to be $\frac{e^2}{\kappa} \frac{V_{\mathrm{imp}}}{z_D} = 0.033$ eV and assume that *some* percent of the ionized donors are generating the disorder potential, that defines the long range fluctuations. In our simulations we perform calculations for a unit cell with areal size of 1.5 μm$\times$1.5 μm which contains 3.3×10^{16} donors per square meters, thus with 10 percent disorder we should have $N_I \sim 3300$ impurities.

Figure 4.4 presents only the long range part of the density fluctuation, when considering 3300 impurities. The arrows show the average distance between two maxima, which is calculated approximately to be 550 nm. To estimate an average range of the disorder potential, we repeated calculations for such randomly distributed impurities, where number of repetitions scales with $\sqrt{N_I}$. Such a statistical investigation, sufficiently ensembles the system to provide a reasonable estimation of the long range fluctuations. We also tested for larger number of random distributions, however, the estimation deviated less than tens of nanometers. We show our main result of this section in Fig. 4.5, where we plot the estimated long range part of the disorder potential considering various number of impurities N_I and impurity potential amplitude V_{imp}. Our first observation is that the long range part of the total potential becomes less when N_I becomes large, not surprisingly. However, the range increases nonlin-
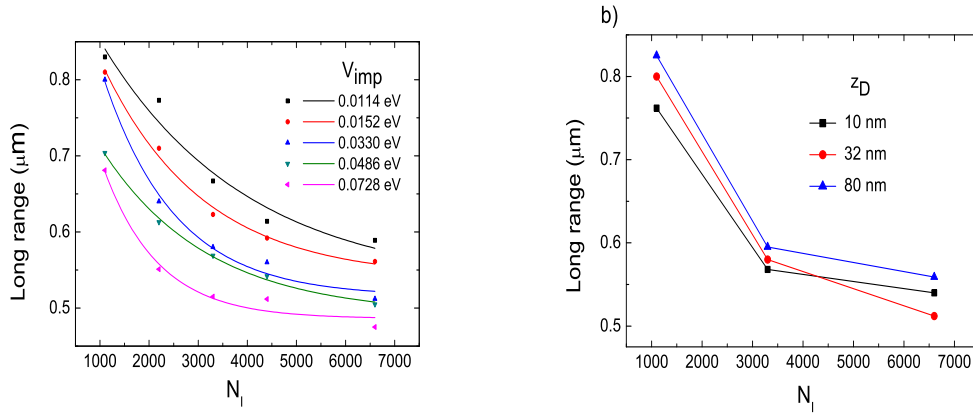
Figure 4.5 Statistically estimated range of the density fluctuations as a function of number of impurities, considering various impurity strengths (a) and spacer thicknesses (b). The calculations are done at zero temperature considering Coulomb impurities. The long range potential fluctuations become larger than the size of the unit cell if one considers less than %5 disorder.

early while decreasing N_I, obeying almost an inverse square law and tend to saturate at highly disordered system. When fixing the distributions and N_I, and changing the amplitude of the impurity potential we observe that for large amplitudes the range can differ as large as 200 nm at all impurity densities. We found that for impurity concentration less than %3, the range of the potential is larger than the unit cell we consider, *i.e* $R > 1.5\mu$m. In contrast to the long range part, the short range part is almost unaffected by the impurity concentration, however, is affected by the amplitude. Therefore, while defining the conductivities we will focus our investigation on V_{imp}. All of the above numerical observations coincide fairly good with our analytical investigations in the previous section. However, the range dependency on the impurity concentration cannot be estimated with the analytical formulas given. We should also note that, similar or even complicated numerical calculations are present in the literature (Nixon, 1990; Stopa, 1996). A indirect measure of the screening effects on the potential can also be inferred by capacitance measurements, supported by the above calculation scheme in the presence of external field (Mares, 2009).

To summarize: we performed 3D numerical calculations to estimate the effect of impurities on the potential landscape experienced by the 2DES. We found that, the range of the fluctuations strongly depend on the number of impurities. If one adds more than % 20 percent of impurity, the range of the potential fluctuations are less than 400-500 nm, however, this (short) range is affected by the amplitude of single impurity potential. Whereas, if only few percent of disorder is considered the range becomes approximately more than 650 nm. In contrast to the highly disordered case, the amplitude of single impurity potential is less pronounced. The spacer thickness seems not to play an important role in defining the range of the potential fluctuations, while keeping V_{imp} constant.

Next section is devoted to investigate the widths of the quantized Hall plateaus utilizing our findings. We consider mainly two "mobility" regimes, where the long range fluctuations is at the order of microns (high mobility) and is at the order of few hundred nanometers, low mobility. However, the amplitude of the total potential fluctuations will be estimated not only depending on the number of impurities but also depending on the spacer thickness, range and amplitude of single impurity potential.

4.3   Quantized Hall Plateaus

The main aim of this section is to provide a systematic investigation of the quantized Hall plateau (QHP) widths within the screening theory of the IQHE (Siddiki, 2004), therefore here we summarize the essential findings of the mentioned theory. In calculating the QHPs one needs to know local conductivities, namely the longitudinal $\sigma_{\mathrm{l}}(x,y)$ and the transverse $\sigma_{\mathrm{H}}(x,y)$. To determine these quantities it is required to relate the electron density distribution $n_{\mathrm{el}}(x,y)$ to the local conductivities explicitly. Here we utilize the SCBA (Ando, 1982). However, the calculation of the electron density and the potential distribution including direct Coulomb interaction is not straightforward, one has to solve the Schrödinger and the Poisson equations simultaneously.

This is done within the Thomas-Fermi approximation which provides the following prescription to calculate the electron density

$$n_{\text{el}}(x,y) = \int dE D(E) \frac{1}{e^{(E_F - V(x,y))/k_B T} + 1},$$ (4.3.1)

where $D(E)$ is the appropriate density of states calculated within the SCBA, where k_B is the Boltzmann constant and T temperature. The total potential is obtained from

$$V(x,y) = \frac{2e^2}{\bar{\kappa}} \int dx dy K(x,y,x',y') n_{\text{el}}(x,y),$$ (4.3.2)

and the Kernel $K(x,y,x',y')$ is the solution of the Poisson equation satisfying the boundary conditions to be discussed next. In the following we assume a translation in

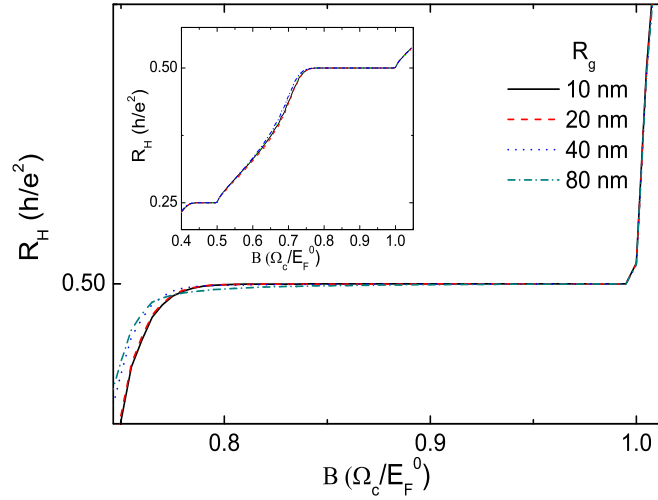

Figure 4.6 The Hall resistances versus magnetic field, calculated at default temperature and considering a 10 μm sample for different ranges of the single impurity potential. Inset depicts a larger B field interval, where also the $v = 4$ plateau can also be observed.

variance in y-direction and implement the boundary conditions $V(-d) = V(d) = 0$ (2d

being the sample width), proposed at Ref. (Chklovskii et al., 1992), such a geometry
allows us to calculate the Kernel in a closed form. Hence, Eqs. (4.3.1) and (4.3.2) can
be rewritten in the self-consistent form as follows

$$V(x) = \frac{2e^2}{\bar{\kappa}} \int_{-d}^{d} dx' \ln \left| \frac{\sqrt{(d^2 - x^2)(d^2 + x^2)} + d^2 - xx'}{(x - x')d} \right| \times \int dE D(E) F[E, k_B T, V(x')],$$
(4.3.3)

where $F(\alpha)$ is the fermi function. For a given initial potential distribution, the elec-
tron concentration can be calculated at finite temperature and magnetic field, where
the density of states $D(E)$ contains the information about the quantizing magnetic
field and the effect of short range impurities. Here we implicitly assume that the elec-
trons reside in the interval $-b < x < b$ (where, $d_l = |d - b|/d$ is called the depletion
length), and is fixed by the Fermi energy, *i.e.* the number of electrons, hence donors.
As a direct consequence of Landau quantization and the locally varying electrostatic
potential, the electronic system is separated into two distinct regions, when solving
the above self-consistent equations iteratively: i) The Fermi energy equals to (spin
degenerate) Landau energy and due to DOS the system illustrates a metallic behavior,
the compressible region, ii) The insulator like incompressible region, where E_F falls
in between two consequent eigen-energies and no states are available (Chklovskii et
al., 1992; Siddiki, 2003). It is usual to define the filling factor ν, to express the elec-
tron density in terms of the applied B field as, $\nu = 2\pi l^2 n_{\text{el}}$. Since all the states below
the Fermi energy are occupied the filling factor of the incompressible regions corre-
spond to integer values (*e.g.* $\nu = 2, 4, 6...$), whereas the compressible regions have
non-integer values, due to partially occupied higher most Landau level. The spatial
distribution and widths of these regions are determined by the confinement potential
(Chklovskii et al., 1992), magnetic field (Lier, 1994), temperature (Oh et al., 1997)
and level broadening (Güven, 2003; Siddiki, 2004). For the purpose of the present
work we fix the confinement potential profile by confining ourselves to the Chklovskii
geometry and keeping the donor concentration (and distribution) constant. Moreover
we perform our calculations at a default temperature given by $k_B T / E_F^0 = 0.02$, where
E_F^0 is the Fermi energy calculated for the electron concentration at the center of the

sample and is typically similar to 10 meV.

The next step is to calculate the global resistances, *i.e.* the longitudinal R_{L} and Hall R_{H} resistances, starting from the local conductivity tensor elements. Such a calculation is done within a relaxed local model that relates the current densities $\mathbf{j}(x,y)$ to the electric fields $\mathbf{E}(x,y)$, namely the local Ohm's law:

$$\mathbf{j}(x,y) = \hat{\sigma}(x,y)\mathbf{E}(x,y). \tag{4.3.4}$$

The strict locality of the conductivity model is lifted by an spatial averaging process (Siddiki, 2004) over the quantum mechanical length scales and an averaged conductivity tensor $\hat{\bar{\sigma}}(x,y)$ is used to obtain the global resistances. It should be emphasized that, such an averaging process also simulates the quantum mechanical effects on the electrostatic quantities. To be explicit: if the widths of the current carrying incompressible strips become narrower than the extend of the wave functions, these strips become "leaky" which can not decouple the two sides of the Hall bar and back-scattering takes place. Therefore, to simulate the "leakiness" of the incompressible strips we perform coarse-graining over quantum mechanical length scales.

Now let us relate the local conductivities with the local filling factors. Since the compressible regions behave like a metal within these regions there is finite scattering leading to finite conductivity. In contrast, within the incompressible regions the back-scattering is absent, hence, the longitudinal conductivity (and simultaneously resistivity) vanishes. Therefore, all the imposed current is confined to these regions. The Hall conductivity, meanwhile is just proportional to the local electron density. The explicit forms of the conductivity tensor elements are presented elsewhere (Siddiki, 2004). Having the electron density and local magneto-transport coefficients at hand, we perform calculations to obtain the widths of the quantized Hall plateaus utilizing the above described, microscopic model assisted by the local Ohm's law at a fixed external current I. Further details of the calculation scheme is reviewed in Ref.

(Gerhardts, 2008).
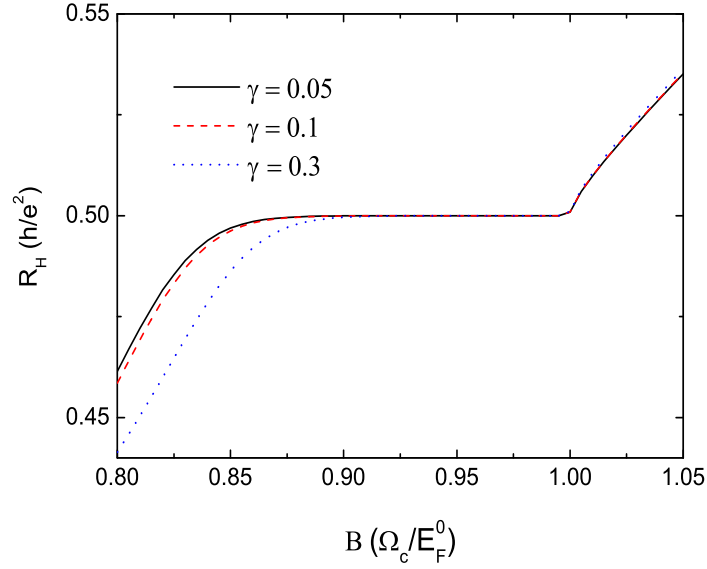
Figure 4.7   The calculated Hall resistances at default temperature assuming a 5 μm sample considering three characteristic value of the broadening parameter. The lowest mobility (γ_I=0.3) shows the narrowest plateau.

4.3.1   Single Impurity Potentials: Level Broadening and Conductivities

Since the very early days of the charge transport theory, collisions played an important role. Such a scattering based definition of conduction also applies for the system at hand, *i.e.* a two-dimensional electron gas subject to perpendicular magnetic field. Among many other approaches (Gerhardts, 1975 ;Güven, 2003; Kramer, 2006) the SCBA emerged as a reasonable model to describe the DOS assuming Gaussian impurities, considering short range scattering. A single impurity has two distinct parameters that represents the properties of the resulting potential, the range R_g (at the order of separation thickness) and the amplitude of the potential (in relevant units), $\widetilde{V}_{imp}$.

$d_l = 70$ nm	$R_g = 10$ nm	20 nm	40 nm	80 nm
2d= 2 μm	0.120	0.120	0.100	0.050
3 μm	0.135	0.125	0.090	0.035
5 μm	0.140	0.115	0.070	0.020
8 μm	0.135	0.095	0.050	0.010
10 μm	0.130	0.085	0.040	0.010

$d_l = 150$ nm	$R_g = 10$ nm	20 nm	40 nm	80 nm
2d= 2 μm	0.140	0.140	0.125	0.075
3 μm	0.160	0.150	0.120	0.055
5 μm	0.180	0.150	0.095	0.035
8 μm	0.180	0.130	0.070	0.020
10 μm	0.175	0.120	0.060	0.015

Table 4.1   The $\nu = 2$ plateau widths obtained at default temperature for two depletion lengths d_l (left 75 nm, right 150 nm), while $\gamma_I = 0.05$ is fixed. The widths are given in units of $\hbar\omega_c/E_F^0 = \Omega_c/E_F^0$.

However, these two parameters are not enough to define the widths of the Landau levels, another important parameter is the number of the impurities, N_I. In the previous section we have already investigated these three parameters in scope of potential landscape, now we utilize our findings to define the level widths and the conductivities. It is more convenient to write the single impurity potential of the form,

$$V_g(r) = \frac{\widetilde{V}_{\text{imp}}}{\pi R_g^2} \exp\left(-\frac{r^2}{R_g^2}\right). \tag{4.3.5}$$

At this point we would like to make a remark on the concepts short/long range impurities and short/long range potential fluctuations, which is commonly mixed. By short range impurity potential we mean that $R_g \lesssim l$, however, by short range potential fluctuation a length scale of the order of $200 - 300$ nm is meant. The long range impurity potential corresponds to $R_g > l$ and long range potential fluctuation is of the order of micrometers. Thus, when considering short range impurities the potential fluctuations may be long range, if N_I is not large ($< \%5$ of the donor concentration). We have also observed that, the long-range potential fluctuations are more efficiently

screened by the 2DES and their range can be at the order of 500 nm at most, when assuming large impurity concentration, *i.e.* $N_I > \%10$.
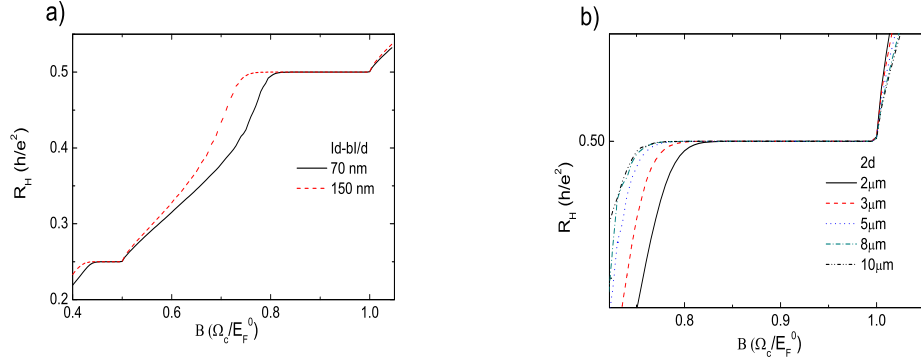

Figure 4.8 a) The calculated Hall resistances at a large B interval at default temperature, setting $2d = 5\ \mu$m, $R_g = 20$ nm and $\gamma_I = 0.05$, while changing the depletion length. It is clearly seen that depletion length is much more important than the single impurity parameters in determining the plateau widths. (b) The direct comparison of the plateau widths considering different sample sizes. The impurity parameters and depletion lengths are kept constant. Calculations are done at $k_BT/E_F^0 = 0.02$, whereas the donor density is 4×10^{15} m^{-2} for all sample sizes.

In light of the above findings and formulation we now investigate the widths of the quantized Hall plateaus. Figure 4.6 presents the calculated Hall resistances at a fixed temperature for typical single impurity ranges. We observe that, when increasing R_g the plateau widths remain approximately the same, with a small variation, which is in contrast to the experimental findings, *i.e.* if the system is low mobility (small $R_g \Rightarrow$ highly broadened DOS) the plateau are larger. In fact changing R_g from 10 nm to 20 nm should increase the zero B field mobility almost an order of magnitude, when fixing the other parameters (see *e.g* table I of Ref. (Siddiki, 2004)). The contradicting behavior is due to the fact that the levels become broader when increasing the single impurity range, therefore the incompressible strips become narrower, which results in a narrower plateau. However, the long range potential fluctuations are completely neglected, therefore the effect(s) of disorder on the quantized Hall plateaus cannot be described in a complete manner. To investigate the effect of the single impurity range

we systematically calculated the plateau widths; table 4.1 depicts the calculated widths of the Hall plateaus considering different sample widths, depletion lengths, filling factors and R_g. One sees that the plateau widths are affected by the increase of impurity range, however, in a completely wrong direction, *i.e.* plateaus become narrower when decreasing the mobility. As we show in the next section, it is not sufficient to describe mobility only considering the range of a single impurity. Moreover, we also show that the other two parameters defining $B = 0$ mobility are either not important or behaves in the opposite direction when calculating the resistances. Next we
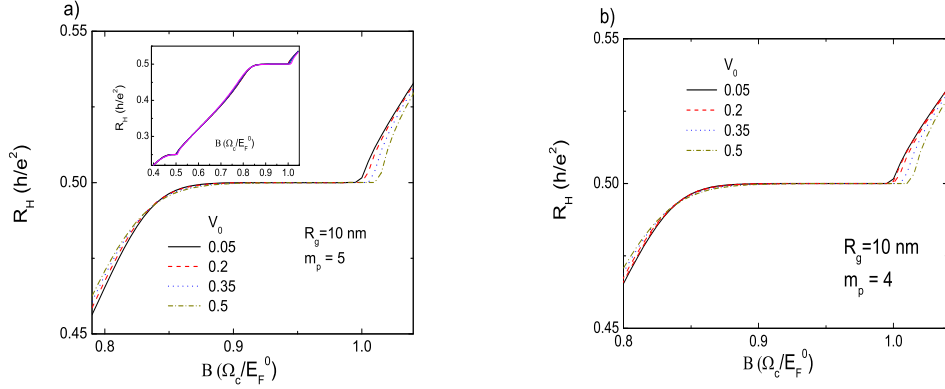

Figure 4.9   Self-consistently obtained Hall resistances for a modulated system considering a sample of 3 μm. The depletion lengths and other single impurity parameters are kept fixed, whereas the parity of the modulation period is odd (a) or even (b).

investigate the effect of the remaining two parameters, $\widetilde{V}_{imp}$ and N_I. However, these two parameters both effect the level width simultaneously, thereby the widths of the incompressible strips. Hence, one cannot to distinguish their influence on the QHPs separately. Typical Hall resistances are shown in Fig. 4.7 calculated at default temperature considering different impurity parameters. Similar to the range parameter, we observe that the plateau widths become narrower when the mobility is low, which also points that our single particle based level broadening calculations are not in the correct direction. Such a behavior is easy to understand, when we decrease the mobility either by increasing the impurity concentration or by the amplitude of the impurity poten-

tial, the Landau levels become broader due to collisions. This means that, both the energetic and spatial gap between two consequent levels is reduced, hence the resulting incompressible strips are also narrower and fragile even at low temperatures. A detailed investigation on the incompressible widths depending on impurity parameters are reported in Ref. (Güven, 2003). It is known that if there exists an incompressible strip wider than the Fermi wavelength the system is in the quantized Hall regime (Siddiki, 2004), therefore, if the gap is reduced the incompressible strips are smeared, thus the quantized Hall plateau vanish. As a general remark on the single particle theories, we should note that such a reduced gap is also a gross problem for the non-interacting models (Laughlin, 1981; Buttiker, 1988; Halperin, 1982), however, one can overcome this discrepancy by making localization assumptions (Kramer, 2003). Namely, one assumes that even within the broadened Landau levels there are states, which are localized, therefore electrons cannot contribute to transport. Hence, although the gap is small (levels are broad) these localized states serves as a reasonable candidate to explain the low mobility behavior. In the early days of IQHE it was a great challenge to describe and observe these localized states (Cai, 1986). Recent experiments (Ahlswede, 2001; Ilani, 2000; Steele, 2005) show clearly that, the localization assumptions are not relevant in all the cases, *i.e.* narrow and high mobility samples. Moreover, the universal behavior of the localization length dictated by these theories fail (Slevin, 2009).

4.3.2   *Size Effects on Plateau Widths*

Another important parameter in defining the plateau widths is the depletion length d_l. The slope of the confinement potential close to the edges essentially determines the widths of the incompressible strips (Chklovskii et al., 1992), which in turn determines the plateau widths. In Fig. 4.8 we show the ν=2 plateau calculated for two different depletion lengths, we see that for the larger depletion the plateau is more extended. Since, the larger the depletion is, the smoother the electron density is. Therefore,
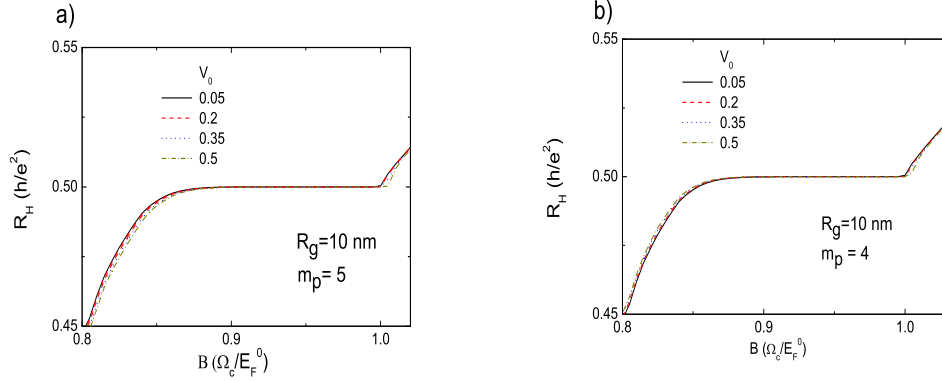
Figure 4.10   The variation of the Hall resistance considering odd (a) and even (b) modulation periods, plotted for characteristic modulation amplitudes. All calculations are performed at the default temperature and the depletion length is fixed to 75 nm. The parameters defining the single impurity potential are kept same, *i.e* $\gamma_I = 0.05$ and $R_g = 10$ nm.

resulting incompressible strips are wider, hence the plateau. Such an argument will fail if one considers a highly disordered large sample, which we discuss in Sec. 4.3.3. Next, we compare the plateau widths of different sample sizes while keeping constant the disorder parameters and depletion length. Figure 4.8 depicts the sample size dependency of $\nu = 2$ plateau width. It is seen that the larger samples present wider plateaus, if the magnetic field is normalized with the center Fermi energy, E_F^0. One can understand this by similar arguments given above, *i.e.* if the sample is narrow the variation of the confinement potential is stronger, therefore the incompressible strips become narrower, hence, the plateaus. The discrepancy between the experimental results and the screening theory of the IQHE is solved if one considers not only the single impurity potentials but also the overall *disorder* potential landscape generated by the impurities. In the next part of this section, we investigate the effect of the long range potential fluctuations on the quantized Hall plateaus and find that, when the mobility is reduced the plateaus become wider and stabile, as it is observed in many experiments, (see *e.g.* Refs. (Haug, 1982; Siddiki et all., 2009).
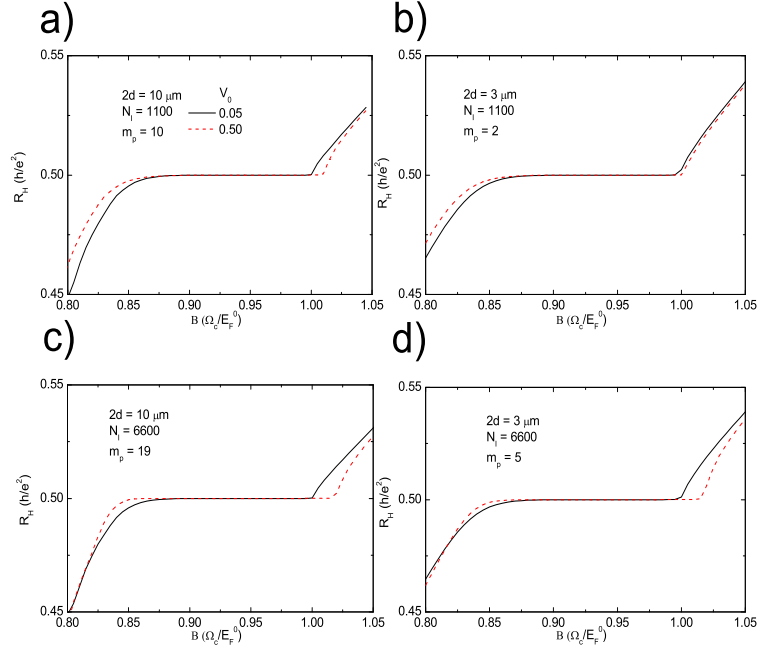
Figure 4.11 Line plots of the Hall resistance as a function of magnetic field considering two sample widths ($2d = 10$ μm left panels, $2d = 3$ μm right panels) and impurity concentrations ($\sim \%3$ (a) and (b), $\sim \%20$ (c) and (d)).

4.3.3 Many Many Impurities: Potential Fluctuations

So far we have investigated the effect of single impurity potentials on the overall potential landscape in Sec. 4.2.3 and on the widths of the plateaus in Sec. 4.3.1. We have seen that, at high impurity concentration the overall potential fluctuates over a length scale of couple of hundred nanometers, whereas for low N_I concentration such length scale can be as large as micrometers. Now we include the effect of this long range potential fluctuations *into* our screening calculations via modulation potential defined as $V_{\mathrm{mod}}(x) = V_0 \cos\left(\frac{2\pi x m_p}{2d}\right)$ where, the modulation period m_p, is chosen such that the boundary conditions are preserved. At the moment, we consider two modulation periods regardless of the sample width and vary the amplitude of the modulation

potential. In the next section, however, we select these two parameters from our estimations obtained in Sec. 4.2 and Sec. 4.2.3.

Figure 4.9a depicts the self-consistently calculated Hall resistances, considering different modulation amplitudes V_0 for a fixed sample width ($2d = 3$ μm) and $m_p = 5$. We observe that, the plateaus become wider from the high B field side, when V_0 is increased, *i.e* mobility is reduced. Such a behavior is now consistent with the experimental findings. Since the QHPs occur whenever an incompressible strip is formed (somewhere) in the sample and the modulation forces the 2DES to form an incompressible strip at a higher magnetic field, therefore the plateau is also extended up to higher field compared with the (approximately) non-modulated calculation, $V_0/E_F^0 < 0.1$. It is important to note that the parity of the modulation period, *i.e* whether m_p is even or odd number of oscillations, does not play an important when considering narrow samples at least for the case under investigation, Fig. 4.9b. However, parity of the modulation period plays a role when one considers a larger sample size ($2d = 10$ μm) or if the period is larger. Next we consider a $2d = 10$ μm sample: The odd m_p ($= 5$) widens the plateau from the high field side (Fig. 4.10a). Whereas for the modulation period $m_p = 4$, the $\nu = 2$ plateau enlarges both from high and low B field, and the center of the plateau is shifted to the high B side, shown in Fig. 4.10b. The extension at the low field edge is due to the formation of wide incompressible strips at the edges of the sample, thus the high temperature resistance crosses the plateau rather at the center. This odd-even effect is discussed later once more.

Our investigation of the impurities lead us to conclude that, one has to define mobility at high magnetic fields also taking into account screening effects in general and furthermore also the geometric properties of the sample such as the width and depletion length. As an example if we consider an impurity concentration of $\approx \%1$ the long range part of the potential fluctuation can be approximated to 900 nm. However, note that the amplitude of this fluctuation varies between $\%5 - 25$ of the Fermi energy, considering different separation thicknesses, therefore the wafer changes from

low mobility to intermediate one. Another important parameter is the number of modulations within the system: a sample with an extend of 2 μm and $V_0/E_F = 0.1$ is a high mobility sample with the same m_p (only 2 maximum), however, sample with a width of 10 μm is low mobility (10 maximum). In the next section we study the plateau widths of different mobility samples, while keeping constant the extend and the amplitude of long range potential fluctuations (*i.e.* V_0 and m_p) and short range impurity parameters ($\widetilde{V}_{\text{imp}}$, N_I and R_g) under experimental conditions.

4.4 Discussion: Comparison with the Experiments

In this final section, we harvest our findings of the previous sections to make quantitative estimations of the plateau widths, considering narrow gate defined samples. Our aim is to show the qualitative and quantitative differences between "high" and "low" mobility samples, by taking into account properties of the single impurity potentials and the resulting disorder potential. The experimental realizations of these samples are reported in the literature (Siddiki et all., 2009). We estimated in Sec. 4.2.3 that, the range of the potential fluctuations is $\lesssim 500$ nm for low mobility ($N_I > 3300$) and is $\gtrsim 1$ μm at high mobility. Therefore, the modulation period is chosen such that many oscillations correspond to low mobility, and few oscillations correspond high mobility. As an specific example let us consider a 10 μm sample, for the low mobility we choose $m_p = 19 - 20$ and for the high mobility m_p is taken as 9 or 10. The amplitude of the disorder potential is damped to %50 of the Fermi energy when considering the effect of spacer thickness, however, including screening this amplitude is further reduced to few percents. In light of this estimations the low mobility will be presented by a modulation amplitude of $V_0/E_F^0 = 0.5$, whereas high mobility corresponds to $V_0/E_F^0 = 0.05$. Therefore, we have 4 different combinations of the disorder potential parameters yielding four different mobilities considering two sample widths, as tabulated in table 4.2. The second important aspect of the disorder is the single impurity parameters, for low mobility set we choose $R_g = 20$ nm and $\gamma_I = 0.3$, whereas

mobility	m_p (10 μm)	m_p (2 μm)	V_0/E_F^0
low	19-20	5-6	0.5
intermediate 1	9-10	2-3	0.5
intermediate 2	19-20	5-6	0.05
high	9-10	2-3	0.05

Table 4.2   A qualitative comparison of the mobility in the presence of magnetic field also taking into account self-consistent screening. Mobility also depends on the size of the sample when screening is also considered.

for high mobility $R_g = 10$ nm and $\gamma_I = 0.05$ is set. Remember that, the range of the single impurity is much less important than γ_I in determining the plateau width (see sec. 4.3.1).
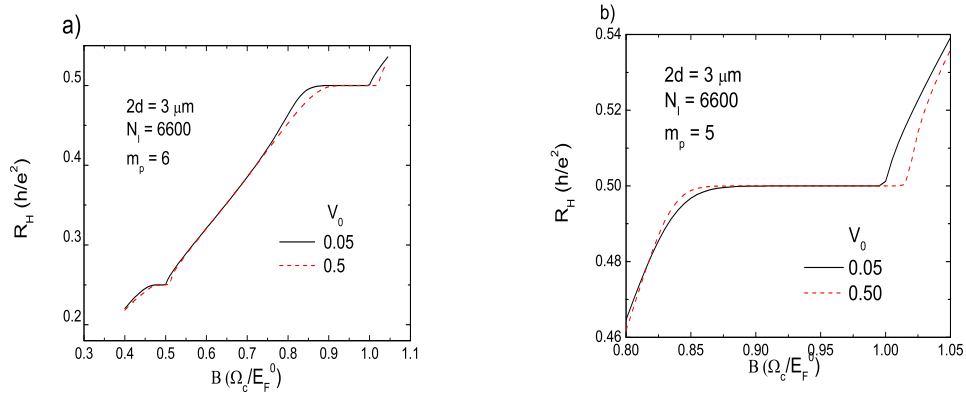

Figure 4.12   Even-odd parity dependency of the Hall plateaus at high impurity concentration. (a) corresponds to a "acceptor" doped wafer, whereas in (b) the ionized impurities are positively charged.

Figure 4.11 summarizes our results considering above discussed mobility regimes for two different sample widths. In Fig. 4.11a, we show the calculated Hall resistances for a sample of 10 microns with the highest mobility (solid (black) line) and intermediate 1 mobility (broken (red) line). The solid line is the highest mobility since the range of the fluctuations are at the order of 1 μm and the amplitude of the modulation potential is five percent of the Fermi energy. The broken line presents the intermediate mobility considering a modulation amplitude of fifty percent. We observe that the lower mobility wafer presents a larger quantized Hall plateau, which is now in com-

plete agreement with the experimental results. Moreover, our calculation scheme is free of localization assumptions in contrast to the known literature and we only considered a very limited level broadening, *i.e.* $\gamma_l = 0.05$. In fact our results also hold for Dirac-delta Landau levels, however, for the sake of consistency we choose the broadening parameters according to the selected disorder parameters. In Fig. 4.11c, we show two curves for even lower mobilities, the solid line corresponds to the intermediate 2 case, whereas the broken line is the lowest mobility considered here. The potential fluctuation range (*i.e.* the modulation period) is chosen to present the low mobility wafer. We again see that for the lowest mobility the quantized Hall plateau is enlarged considerably from both edges of the plateau. These results explicitly show that the quantized Hall plateaus become broader if one strongly modulates the electronic system by long range potential fluctuations, either by changing the range *or* the amplitude of the modulation. Similar results are also obtained for a relatively narrower sample $2d = 3$ μm, Fig. 4.11b and 4.11d, however, we see that decreasing the range of the potential fluctuation is more efficient in enlarging the quantized Hall plateaus when compared to the effect of the amplitude of the modulation.

The last interesting investigation is on the parity of the modulation period, *i.e.* whether m_p is odd or even. Figure 4.12 presents the different behavior when considering even (a) or odd (b) periods. Here, all the disorder parameters are kept fixed, other than the parity. We see that for the even parity the plateau is shifted towards the high field edge, both for $v = 2$ and 4, whereas for the odd parity the plateau is enlarged from both sides. This tendency is also observed for the larger sample (not shown here). We attribute this behavior again to the formation of the incompressible strips, however, this time only to the one residing at the center of the sample, *i.e.* the bulk incompressible strip. The picture is as follows: If the maxima of the modulation potential is at the center of the sample, the incompressible strip is formed at a higher magnetic field value, whereas, the edge incompressible strips become narrower at the lower field side. Hence, due to the larger incompressible strip at the bulk of the sample the plateau is shifted to the higher field, in contrast, due to the narrower (compared

to the unmodulated system) edge strips the plateau is cut off at higher fields. Since, the edge incompressible strip becomes narrower than the extend of the wave function. For the odd parity, the edge incompressible strips become wider, therefore, the plateau extends to the lower B fields. The enhancement at the high field edge results from the two maximum in the proximity of the center. For a better visualization of the incompressible strip distribution we suggest reader to look at Fig.2 of Ref.(Siddiki, 2007) and Fig.1 of Ref. (Siddiki, 2002). Such a shift of the quantized Hall plateaus is also reported in the literature (Haug, 1982). We claim that, the shift due to the modulation parity change observed in our calculations overlap with their findings. Note that in our calculations we only consider symmetric DOS, however, replacing a maxima with a minima at the confinement potential corresponds to the acceptor behavior of the dopants. A systematic experimental investigation is suggested to understand the underlying physical mechanism, where the system is doped with small number of acceptors.

In summary, we tackled with the long standing and widely discussed question of the effect of disorder on the quantized Hall plateaus. The distinguishing aspect of our approach relies on the separate treatment of the long and short range of the disorder potential. We show that assuming Gaussian impurities is not sufficient to describe long range potential fluctuations, however, is adequate to give a prescription in defining the density of states broadening and conductivities. The discrepancy in handling the long range potential fluctuations is cured by the inclusion of a modulation potential to the self-consistent calculations. We estimated the range of these fluctuations from our analytical and numerical calculations considering the effect of dielectric spacer and the screening of the 2DES. It is observed that spacer damps the short range fluctuations effectively, whereas the direct Coulomb interaction is dominant in screening the long range fluctuations. Utilizing the estimations of the range and the amplitude of potential fluctuations, we classified mobility in four groups and calculated the Hall resistances within the screening theory of the quantized Hall effect. We found that the Hall plateaus are wider when decreasing the mobility, not surprisingly. However, the

most important point of our theory is that, we do not consider any localization assumptions and can still obtain correct behavior of the plateau widths. We show that $B = 0$ and/or short range impurity defined mobility is not adequate to describe the actual mobility at high magnetic fields, moreover, one has to include geometrical properties of the sample at hand.

CHAPTER FIVE
EVANESCENT INCOMPRESSIBLE STRIPS AS ORIGIN OF THE OBSERVED HALL RESISTANCE OVERSHOOT

5.1 Introduction

One of the most commonly used material characterization method is to measure the resistance of the sample. The Hall resistivity is linear in B for a typical three-dimensional materials, which is drastically altered at two-dimensional systems to a stepwise behavior. This phenomenon is known as the integer quantized Hall effect (IQHE) (Klitzing, 1980). However, non-monotonic anomalous peaks at the low B side of the plateaus are also reported in many different materials and are discussed in a fairly varying contexts (Richter, 1992; Ramvall, 1998; Griffin, 2007; Shlimak, 2005; Shlimak, 2006). The non-monotonic increase of the Hall resistance is known as the overshoot, and is usually attributed to impurity effects, similar to IQHE. Recently, resistance overshoot is experimentally investigated in relatively narrow samples and the results are discussed in the context of interaction induced incompressible strips in a phenomenological manner (Sailer, 2010). We present our results that provide a self-consistent calculation (Siddiki, 2004; Guven, 2003) scheme to explain the observed resistance overshoot. First, we discuss the formation of the compressible and incompressible strips an analytical description. We show that, under certain conditions evanescent incompressible strips assuming different filling factors can co-exist and contribute to the current, hence Hall resistance. Later, we calculate Hall resistances within a local version of the Ohm's law and numerically investigate the dependencies of the overshoot on disorder and sample size. Finally, we predict that the resistance overshoot can be manipulated by changing the edge profile of the system.

5.1.1 *The Semi-classical Model*

In this section we investigated the formation and deformation of the incompressible strips within the frame work of Chklovskii et. al. and Siddiki et. al., respectively. The

earlier work is constructed on the electrostatic equilibrium condition of the 2DEG in the presence of an external B field. It is assumed that the 2DES resides on the $z = 0$ plane, confined by an electrostatic potential due to a homogeneous donor layer with a constant density n_0 and the electrons are depleted from the edges by an amount of ℓ_d, by the virtue of metallic in-plane gates. Translation invariance is imposed in the y direction. In this case, an electron density distribution of the form

$$n_{\text{el}}(x) = \left(\frac{x - l_d}{x + l_d} \right)^{1/2} n_0. \tag{5.1.1}$$

It can be shown that, incompressible strip should form in the vicinity of x_k, which is determined by the condition $k = 2\pi l^2 n_{\text{el}}(x_k)$, k being an integer. The incompressible strip is electrostatically unstable if one neglects electron-electron interactions, the stability condition yields a finite width of the strip given by

$$a_k = \left(\frac{2\kappa\Delta E}{\pi^2 e^2 \frac{dn_{\text{el}}(x)}{dx}|_{x_k}} \right)^{1/2}, \tag{5.1.2}$$

where κ is the dielectric constant of the material and ΔE is determined by the single particle energy gap. The gap can be either the Landau ($\hbar\omega_c$) or Zeeman ($g^*\mu_B B$) gap, where $\omega_c = eB/m$ is the cyclotron frequency and μ_B is the Bohr magneton together with the effective g^* factor. We specify the strength of the gap by $\alpha = g^*\mu_B B/\hbar\omega_c$, if the gap is due to Zeeman splitting; otherwise is given by 1-α. Note that, at Si/SiGe hetero-structures an additional gap exists due to valley degeneracy. Although, the above non-self-consistent scheme seems to be reasonable in handling the electrostatics of the 2DES, numerical self-consistent calculations show that the Chklovskii picture fails to describe the electron distribution (Oh et al., 1997; Siddiki et all., 2009). This is due to the oversimplified assumptions of boundary conditions and essentially is due to the fact that the 2DES is by no means a perfect metal, as considered at the mentioned work. Even utilizing the above boundary conditions, self-consistency alters
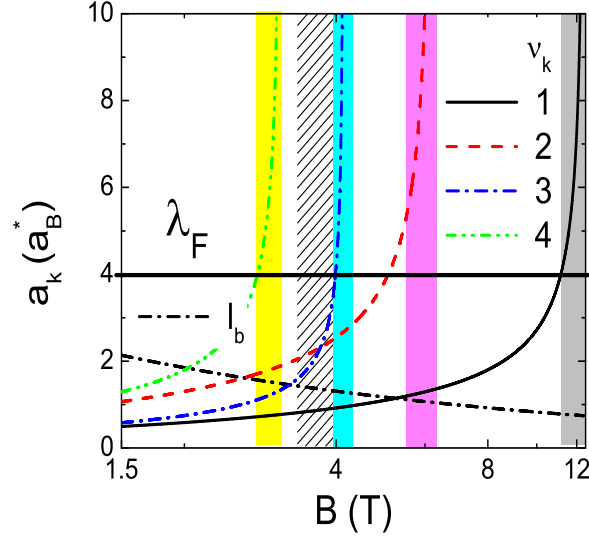
Figure 5.1 Analytically calculated incompressible widths in units of a_B^* (≈ 9.81 nm for GaAs). The Fermi wavelength λ_F considering a typical density of 3×10^{15} m^{-2}, horizontal line. The shaded boxes indicate the quantized Hall interval, whereas diagonally shaded region depicts the overshoot interval. We set $t = 7\,a_B^*$ and $l_d = 20a_B^*$, leading similar results with the self-consistent calculations.

the estimated positions and the widths strongly (Siddiki, 2004). We will re-present the self-consistency below. However, with a slight modification of the density distribution inspired by the self-consistent calculations one can still obtain the widths that coincide with the experimental findings (Siddiki, 2010). We describe the electron density by

$$n_{\mathrm{el}}(x) = (1 - e^{-(x - l_d)/t})n_0, \tag{5.1.3}$$

where t determines the width of the electron poor region in front of the metallic contacts. The widths can be obtained as

$$a_k = \sqrt{\frac{4a_B^* \alpha}{\pi \nu_0} \frac{t}{e^{-(x_k - l_d)/t}}}, \tag{5.1.4}$$
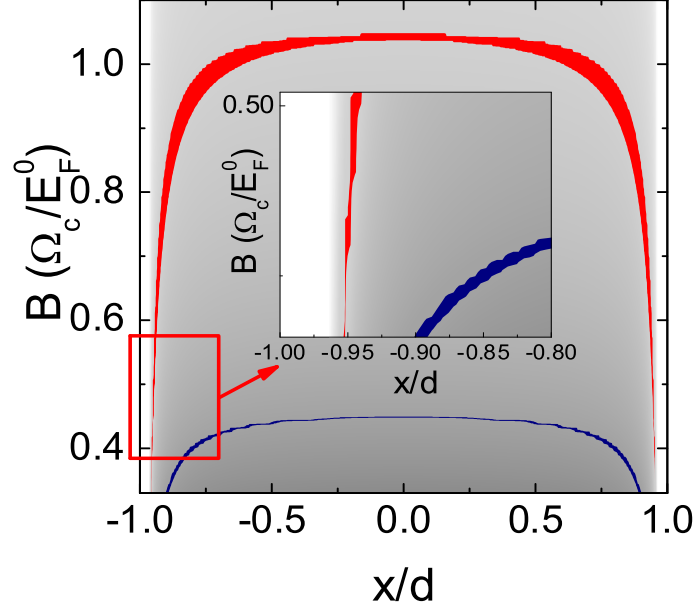
Figure 5.2 The evolution of the incompressible strips as a function of normalized lateral coordinate (horizontal axis) and B field (vertical axis), considering $v = 2$ dark (red) and $v = 4$ darker (blue). We set $l_d/d = 0.02$, where $d = 10\ \mu$m, at default temperature $\Theta_d = kT/E_F^0 = 0.01$. Inset depicts the overlap region.

a_B^* being the effective Bohr radius.

In Fig. 5.1, we show the calculated widths of the incompressible strips with $v = 1..4$, considering a fixed width of the electron poor region and an effective g^*, enhanced by the exchange interactions. We observe that more than one incompressible strip with different v can co-exist below $v = 2$, which we will reconsider their evanescent properties later. For the moment, we would like to calculate the amount of current confined to these strips. Note that, within the incompressible strips the drift velocity ($v_d(x) \propto \mathbf{E} \times \mathbf{B}$) is finite, whereas at the compressible strips it is zero, since the Hall field $E_H(x)$ equals to zero, due to perfect screening. Then, the current density can be calculated via $j_y(x) = -en_{\text{el}}(x)v_d(x)$. Recall that, the electron density is constant within the strip, whereas $v_d(x)$ is determined by the electrochemical potential difference between the source and drain contacts. Hence, one can write the total

current carried by the strip k as

$$I_k = \int_{-a_k/2}^{a_k/2} j_y^k(x)dx = \frac{e}{2\pi}\frac{keB}{m}. \tag{5.1.5}$$

Now to determine the Hall voltage, one should also know the local conductivities. The longitudinal resistivity (or resistance if a square geometry is assumed) is given by

$$\rho_l(x) = \frac{1}{\left(\sigma_l(x) + \sigma_H^2(x)/\sigma_l(x)\right)}, \tag{5.1.6}$$

since the longitudinal conductivity $\sigma_l(x)$ goes to zero at the incompressible strip (Ando, 1982) and Hall conductivity $\sigma_H(x) = \frac{e^2}{h}\nu(x)$, the only contribution to the Hall voltage comes from this region (Siddiki, 2004). The only unresolved problem is now to obtain the quantized Hall voltage, which is not the case if $k > 2$ since it equals to

$$V_H = \frac{e^2}{h}\sum_k I_k/k, \tag{5.1.7}$$

which is not quantized at all. Now we should reconsider the existence of more than one incompressible strip assuming different integer filling factors. In fact, having many incompressible strips is due to an artefact of the Thomas-Fermi approximation which fails to describe the electronic system at hand (Suzuki, 1993; Siddiki, 2004). If one considers the finite size of the wave-functions, together with the limitations of the Fermi distribution function at small systems, one immediately notices that if the incompressible strip becomes narrower than the Fermi wavelength it is no-longer a perfect channel without backscattering, *i.e.* $\sigma_l \neq 0$. Hence, only the incompressible strip having a width larger than the Fermi wavelength λ_F can carry current. In Fig. 5.1, we also show the Fermi wavelength to distinguish the evanescent incompressible strips ($a_k < \lambda_F$) from the well developed ones. Now we can say that, if there exists an incompressible strip larger than λ_F, the Hall potential is quantized. We denote these

intervals by shaded areas in Fig. 5.1. If a_k becomes smaller than the magnetic length, then the system becomes fully classical and is simply described by the well known Drude formalism (Siddiki, 2010). The interesting transition takes place when the condition $l < a_k < \lambda_F$ is satisfied. In this situation, most of the current is flowing from the evanescent incompressible strip, with some background current spread all over the sample. In typical samples, due to the strong confinement at the edges or due to the strong disorder potential fluctuations, these evanescent incompressible strips immediately vanish, just after the quantized Hall plateau disappears. However, there might be cases where two or more of these evanescent strips survive and co-exist, satisfying $l_b < a_k < a_{k+1}... < \lambda_F$. Such a situation is also observed in Fig. 5.1, where $v = 2$ and $v = 3$ incompressible strips co-exist. For this case the Hall resistance will be given by

$$R_H = \frac{h}{e^2}(1/3 + I_2/I(1/2 + 1/3)), \qquad (5.1.8)$$

satisfying the current conservation, namely $I = I_2 + I_3$. The second term in the bracket reflects the contribution to the current from the $v = 2$ evanescent incompressible strip and one can easily see that, the Hall resistance is higher than the quantized value of $\frac{h}{3e^2}$. This is exactly the case of the resistance overshoot: it occurs at the lower B side of the plateau and strongly depends on the system parameters like the Fermi wavelength and geometry (edge profile) (Shlimak, 2005; Sailer, 2010). Having determined the conditions to observe overshoot depending on the existence and properties of the incompressible strips, next, we investigate overshoot within the framework of interaction theory of the quantized Hall effect.

Fig. 5.2 depicts the calculated filling factor distribution as a function of normalized spatial coordinate x/d and external field B expressed in units of $\Omega_c/E_F^0 = \hbar\omega_c/E_F^0$, where E_F^0 is the Fermi energy at the center of the sample. The dark colored croissant like areas highlight the distribution of the incompressible strips. One can see that, two evanescent incompressible strips with different filling factors, namely $v = 2$ and 4, co-exist in the interval $0.4 < B < 0.48$. In the following, we will focus on such

intervals to seek resistance overshoot.

Starting from the self-consistent quantities we calculate the current distribution within the local Ohm's law, relating the local electric field $\vec{E}(x,y)$ to the current density $\vec{j}(x,y)$ via $\vec{E}(x,y) = \hat{\sigma}(x,y)\vec{j}(x,y)$. A typical current distribution is shown in Fig. 5.3 considering three characteristic B field values, where a) most of the current is confined to the inner strip b) the current is shared by both strips, however, flows mainly from the inner strip and c) the current is almost equally confined to both strips. We would expect to have resistance overshoot in cases b) and c), whereas a) would present the classical Hall effect.

We depict the calculated Hall resistance as a function of B in Fig. 5.4, here we consider two different depletion length and calculations are performed at various R. One can clearly see the overshoot at the expected B intervals. The disorder potential leads to an increase in magnitude of the DOS peak. Thus, the energy narrows between two Landau levels. If R increases, the peaks disappear. So, electron distribution disappears in the center of the sample and there is a unique incompressible strip at each edge as shown in Fig. 5.4.

We finalize our discussion, by presenting the effects of the impurity strength on the overshoot in Fig. 5.5. Remarkably, the disorder has a minor influence on the amplitude of the overshoot, which is seen by the weak dependence of the peak depending on γ_I. This is mainly due to the fact that, the impurities only shrink the widths of the evanescent incompressible strips via level broadening. However, it's effect negligible when compared to the role of temperature. It is important to note that, we did not include the long-range potential variations to our screening calculations, which are known to be influential in determining the position and stability of the quantized Hall plateaus (Siddiki, 2007). The effects resulting from long-range fluctuations is an open question, which we would like to attack in the near future.

To summarize, we have shown that the resistance overshoot can be obtained within the framework of self-consistent screening theory. This calculation scheme allows us to investigate the effects of various experimental parameters on the overshoot. It is observed that, the overshoot depends on R, in contrast, is immune to short-range impurity scattering. From our sample width dependent calculations, we conclude that if the edge effects are dominant the overshoot is enhanced. Explicitly, for the large samples disorder effects become more important and overshoot duo to edge effects tends to disappear.

5.2   Predictions and Conclusions

In the light of above results and discussions we predict that, for the smooth edge defined samples the overshoot effect should be enhanced. The reason is: To have co-existing evanescent incompressible strips the condition $l_b < a_k, a_{k+1} < \lambda_F$ should be satisfied, this can only happen if the electron density varies slowly, so that the derivative in Eq. 5.1.4 becomes small. Hence the strip becomes large. The experimental test can be as follows, one can define two narrow (*e.g.* $2d \sim 10\ \mu$m) Hall bars residing parallel to each other, where one of the Hall bars is defined by shallow etching and the other by deep etching. Since, in principle, all the intrinsic properties of the material would be the same for both samples the observed difference at the overshoots (enhanced at the shallow sample) would point out the effects due to the formation of wide evanescent incompressible strips. A gate defined sample can be utilized as well, similar to the ones reported in the literature (Siddiki, 2009; Horas, 2008).
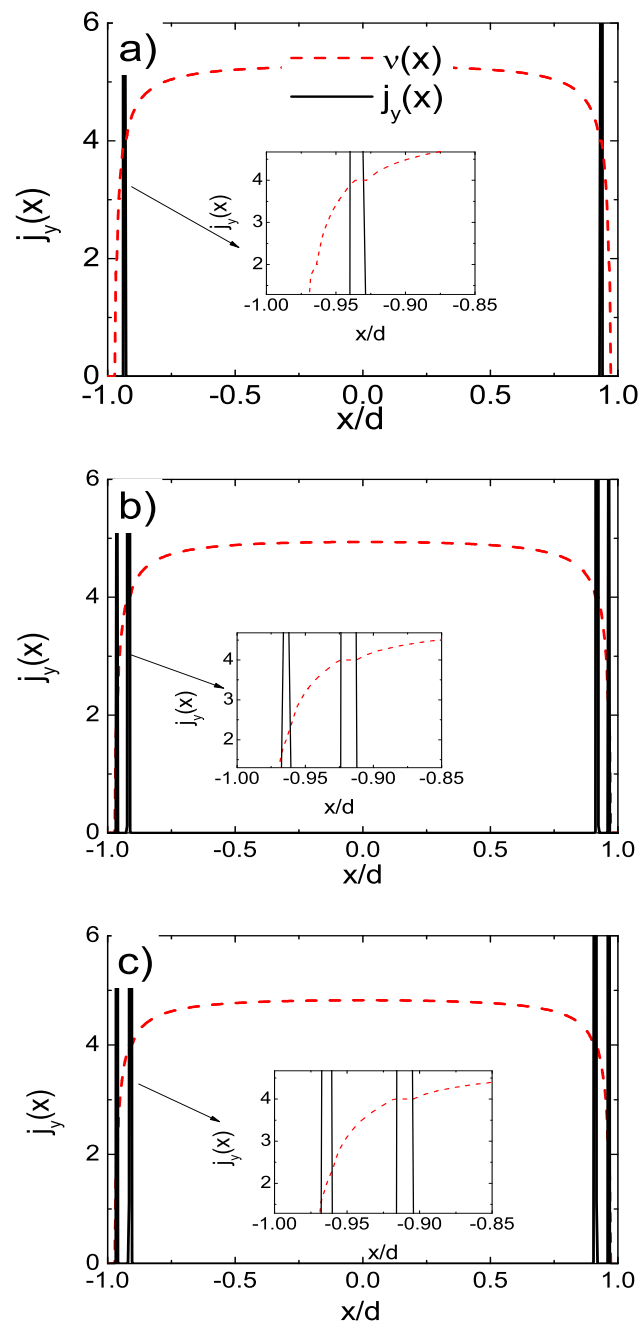
Figure 5.3 The current density (solid line) and filling factor distribution (broken line) as a function of lateral coordinate, calculated at (a) B=0.38, (b) 0.405 and (c) 4.15. Considering default temperature and same parameters in Fig. 5.2.
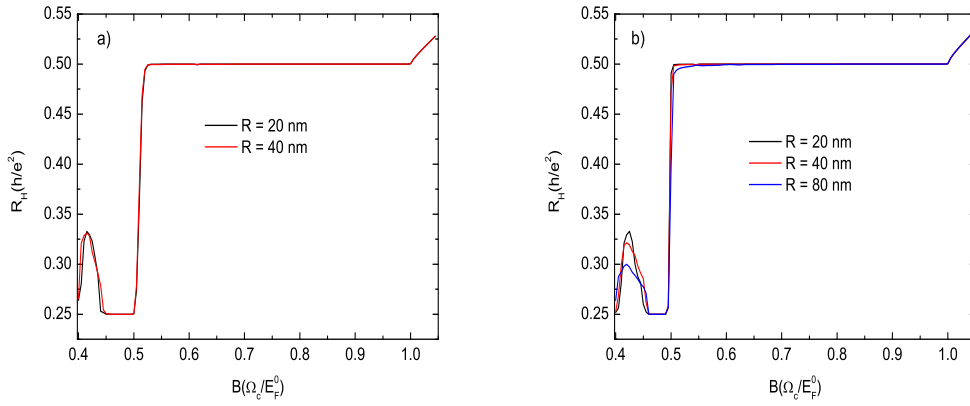
Figure 5.4   Magnetic field dependence of the Hall resistance R_H at different scaled $R\ T = 0.01(k_B T/E_F^0)$ with the depletion length of (a) 70nm and (b) 150nm, $\gamma_I = 0.1$, $2d = 10\mu m$.
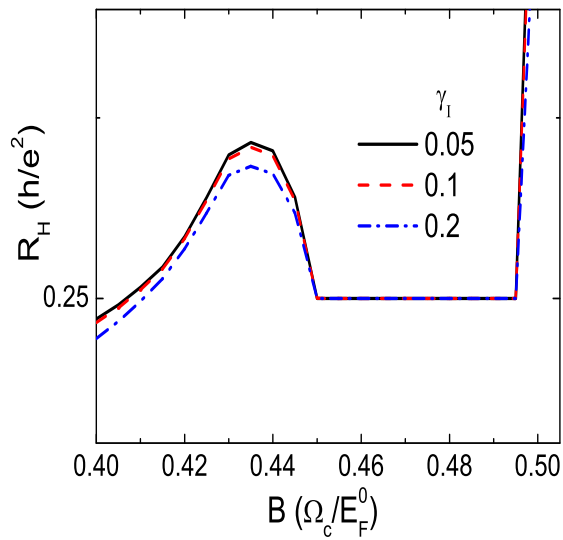

Figure 5.5   Hall resistance versus magnetic field, calculated for different level broadening γ_I considering an 4 μm wide sample at default temperature and depletion length.

CHAPTER SIX
CONCLUSION

The main aim of this thesis is to investigate the effect of disorder and overshooting in the two-dimensional electron system under the QHE conditions. The calculations were done with the semi-classical model Thomas Fermi Approximation, which is much simpler than the corresponding quantum calculations.

This thesis includes two main parts. In the first part of the thesis, we have investigated the effect of disorder potential on the integer quantized Hall effect within the screening theory, systematically. The long ($\gtrsim 1\mu$m) and the short (few hundred nanometers) range potential fluctuations are examined separately. Short range part of the single impurity potential is used to define the conductivity tensor elements within the self-consistent Born approximation. The long range part is treated self-consistently solving the Poisson and Schrödinger equations at the Hartree level. Using the simple, however, fundamental Thomas-Fermi screening, we find that the long range disorder potential is well screened. While, the short range part is approximately unaffected by screening and is suitable to define the mobility at vanishing and finite magnetic fields. In light of these range dependencies we discuss the extend of the quantized Hall plateaus considering *the* "mobility" of the wafer and the width of the sample, by re-formulating the Ohm's law at low temperatures and high magnetic fields. The obtained results could be summarized as follows, our results is that the plateau widths mainly depend on the long range fluctuations of the disorder, whereas the importance of density of states broadening is less pronounced and even is predominantly suppressed. Second one is that we demonstrate that the widths of the quantized Hall plateaus increase with increasing disorder without any localization assumptions.

In the second part of our study, we use a semi-analytical model, based on the screening theory of the Integer Quantized Hall Effect (IQHE) to investigate the sample width, depletion length and disorder effects on the form of the anomalous, i.e. overshoot Hall resistance R_H, under varying magnetic field. The overshoot of the quantized

Hall resistance is observed at low magnetic field edge of the plateaus. However, if the magnetic field increases further, R_H decreases to its normal value. The effects of the sample width, disorder strength and magnetic field on the overshoot peaks are investigated in detail. The obtained results could be summarized as follows: First one of these results show that the overshoot resistance as a function of magnetic field depends strongly on the edge electrostatics of the sample. From our sample width dependent calculations, we conclude that if the edge effects are dominant the overshoot is enhanced. Explicitly, for the large samples disorder effects become more important and overshoot tends to disappear.

As a summary of these investigations were dedicated to search the role of the disorder effect on a two dimensional electron gas in the presence of a strong perpendicular magnetic fields by using Thomas Fermi Approximation and to analyze the overshoot resistance for the GaAs/GaAlAs heterojunction with regard to the disorder, magnetic field and sample width effects. The distinguishing part of these works relies on the fact that, without any complicated numerical or analytical methods we can obtain the integer quantized Hall plateaus in a good qualitative agreement with the experiments.

REFERENCES

Abramowitz, M., & Stegun, I. A. (1964). in *Handbook of Mathematical Functions* Dover Publications, New York.

Ahlswede, E., Weitz, P., Weis, J., Klitzing, K. v., & Eberl, K. (2001).Hall potential profiles in the quantum Hall regime measured by a scanning force microscope. *Physica B*, *298*, 562-566.

Ahlswede, E., Weitz, P., Weis, J., Klitzing, K. v., & Eberl, K. (2002). Hall potential distribution in the quantum Hall regime in the vicinity of a potential probe contact. *Physica E 12*, 165-168.

Ahlswede, E. (2002). Potential- und Stromverteilung beim Quantum-Hall-Effekt bestimmt mittels Rasterkraftmikroskopie, PhD thesis, *Max-Planck-Institut fur Festkorperforschung / University of Stuttgart* .

Ando, T., Fowler A. B., & Stern, F. (1982). Electronic properties of two dimensional systems. *Rev. Mod. Phys.*, *54 (2)*, 437-672.

Ando, T., Matsumoto, Y., & Uemura, Y., (1975). Theory of Hall Effect in a Two-Dimensional Electron System. *J. Phys. Soc. Japan*, *39 (2)*, 279-288.

Ando, T., & Uemura Y., (1974). Theory of Oscillatory g Factor in an MOS Inversion Layer under Strong Magnetic Fields, *J. Phys. Soc. Jpn.*, *37 (4)*, 1044-1052.

Arfken, G.B., & Weber, H.J. 1995. *Mathematical Methods For Physicists*, Academic Press, 766-775.

Arslan, S., Cicek, E., Eksi, D., Aktas, S., Weichselbaum, A., & Siddiki, A. (2008). Modeling of quantum point contacts in high magnetic fields and with current bias outside the linear response regime. *Phys. Rev. B*, *78 (12)*, 125423/1-15.

Bachmair, H., Göbel, E. O., Hein, G., Melcher, J., Schumacher, B., Schurr, J., Schweitzer, L, & Warnecke, P. (2003). The von Klitzing resistance standard. *Physica E*, *20 (1-2)*, 14-23.

Bangert, E. (1968). *Z. Physik 215*, 177.

Büttiker, M. (1986). Four-Terminal Phase-Coherent Conductance. *Phys. Rev. Lett. 57* 1761û1764.

Büttiker, M. (1988). Absence of Backscattering in the Quantum Hall Effect in Multi-probe Conductors. *Phys. Rev. B*, *38 (14)*, 9375-9389.

Cai, W., & Ting, C.S. (1986). Screening effect on the Landau-level broadening for electrons in $GaAs - Ga_{1-x}Al_xAs$ heterojunctions. *Phys. Rev. B 33*, 3967û3972.

Champel, T., Florens, S., & Canet, L. (2008). Microscopics of disordered two-dimensional electron gases under high magnetic fields: Equilibrium properties and dissipation in the hydrodynamic regime. *Phys. Rev. B 78 (12)*, 125302-125326.

Chang, A. M. (1990). *Solid State Commun. 74* , 871.

Chklovskii, D. B., Matveev, K. A., & Shklovskii, B. I. (1993). Ballistic conductance of interacting electrons in the quantum Hall regime. *Phys. Rev. B*, *47 (19)*, 12605-12617.

Chklovskii, D. B., Shklovskii, B. I., & Glazman, L. I. (1992). Electrostatics of edge channels. *Phys. Rev. B*, *46 (7)*, 4026-4034.

Datta, S. (1995). *Electronic Transport in Mesoscopic systems* (1th ed.). Cambridge: Cambridge University. Press.

Dahlem, F. (2008). *Adiabatic transport in the quantum Hall regime: Comparison between transport and scanning force microscopy investigations* (Thesis). Max-Planck-Institut Für Festkörperforschung Stuttgart.

Eaves, L., & Sheard, F. W. (1986). Size-dependent quantised breakdown of the dissipationless quantum Hall effect in narrow channels. *Semicond. Sci. Technol. 1*, 346.

Efros, A. L. (1988). Non-Linear screening and the background density of 2DEG states in magnetic field. *Solid State Commun.*, 67 (11), 1019-1022.

Efros, A.L. (1988). *Solid State Commun. 65*, 1281.

Fogler, M.M., & Shklovskii, B.I. (1994). Resistance of a long wire in the quantum Hall regime. *Phys. Rev. B. 50*, 1656-1662.

Gerhardts, R. R.(2008). The effect of screening on current distribution and conductance quantisation in narrow quantum Hall systems. *Physica Status Solidi (b), 245 (2)*, 378-392.

Gerhardts, R.R. (1975). Path-Integral Approach to the Two-Dimensional Magneto-Conductivity Problem: I. General Formulation of the Approach; II. Application to n-Type (100)-Surface Inversion Layers of p-Silicon. *Z. Physik B 21*, 285.

Gerhardts, R.R. (1975). Self-Consistent Transport Equations for Electron-Impurity Systems in a Magnetic Field. *Z. Physik B 22*, 327.

Greshnov, A.A., & Zegrya, G.G. (2007). Integer quantum Hall effect and correlated disorder. *Semiconductors 41*, 1329.

Griffin, N., Dunford, R.B., Pepper, M., Robbins, D.J., Churchill, A. C., & Leong, W. Y. (2000). *J. Phys-Condens. Mat. 12*, 1811.

Güven, K., Gerhardts, R. R., Kaya, I. I., Sağol, B. E., & Nachtwei, G. (2002). Two-level model for the generation and relaxation of hot electrons near the breakdown of the quantum Hall effect. *Phys. Rev. B*, 65 (15), 155316/1-8.

Güven K., & Gerhardts, R. R. (2003). Self-consistent local equilibrium model for density profile and distribution of dissipative currents in a Hall bar under strong magnetic fields. *Phys. Rev. B*, 67 (11), 115327/1-8.

Galistu, G. M. (2010). *Magnetotransport studies of the single and bilayer two dimensional electron gas in the quantum Hall regime.* Universiteit van Amsterdam.

Halperin, B. I. (1982). Quantized Hall conductance, current-carrying edge states, and the existence of extended states in a two-dimensional disordered potential. *Phys. Rev. B, 25 (4)*, 2185-2190.

Haug, R.J., Klitzing, K.V., & Ploog, K. (1987). Analysis of the asymmetry in Shubnikovûde Haas oscillations of two-dimensional systems. *Phys. Rev. B 35*, 5933-5935.

Haug, R.J., Gerhardts, R.R., Klitzing, K.V., & Ploog, K. (1987). Effect of repulsive and attractive scattering centers on the magnetotransport properties of a two-dimensional electron gas. *Physical Review Letters 59*, 1349-1352.

Horas, J., Siddiki, A., Moser, J., Wegscheider, W., & Ludwig, S. (2008). Investigations on unconventional aspects in the quantum Hall regime of narrow gate defined channels. *Physica E 40*, 1130-1132.

Huckestein, B. (1995) *Rev. Mod. Phys. 67*, 357 .

Hwang, E.H., & Das Sarma, S. (2008). Limit to two-dimensional mobility in modulation-doped GaAs quantum structures: How to achieve a mobility of 100 million. *Phys. Rev. B 77(23)*, 235437-235443.

Ilani, S., Yacoby, A., Mahalu, D., & Shtrikman, H. (2000). Unexpected Behavior of the Local Compressibility near the B = 0 Metal-Insulator Transition. *Phys. Rev. Lett. 84*, 3133-3136.

Keiter, H. (1967). Z Physik *198* 215.

Klitzing, K. v., Dorda, G., & Pepper, M. (1980). New Method for High-Accuracy Determination of the Fine-Structure Constant Based on Quantized Hall Resistance. *Phys. Rev. Lett. 45*, 494-497.

Kramer, T. (2006). A heuristic quantum theory of the integer quantum Hall effect. *International Journal of Modern Physics B 20*, 1243-1260.

Kramer, T., Bracher, C., & Kleber, M. (2004). Electron propagation in crossed magnetic and electric fields. *Journal of Optics B: Quantum and Semiclassical Optics 6*, 21-27.

Kramer, B., Kettemann, S., & Ohtsuki, T. (2003). Localization in the quantum Hall regime. *Physica E 20*, 172-187.

Jain, J. K., & Kivelson, S. A. (1988) Quantum Hall effect in quasi one-dimensional systems: resistance fluctuations and breakdown *Phys. Rev. Lett.* 60, 1542û5.

Jain, J. K., & Kivelson, S. A. (1988) The quantum Hall effect as an electrical resistance standard *Rep. Prog. Phys. 60*, 1542û5.

Jeckelmann, B., & Jeanneret, B. (2001) Spatial variation of currents and fields due to localized scatterers in metallic conduction IBM *J. Res. Dev.* 64 1603-1655.

Laughlin, R. B. (1981). Quantized Hall conductivity in two dimensions. *Phys. Rev. B, 23 (10)*, 5632-5633.

Laughlin, R. B. *Rev. Mod. Phys.* 71 (1999) 863.

Lier, K., & Gerhardts, R. R. (1994). Self-consistent calculations of edge channels in laterally confined two-dimensional electron systems. *Phys. Rev. B, 50 (11)*, 7757-7767.

MacLeod, S.J., Chan, K., Martin, T.P., Hamilton, A.R., See, A., Micolich, A.P., Aagesen, M., & Lindelof, P.E. (2009). Role of background impurities in the single-particle relaxation lifetime of a two-dimensional electron gas. *Phys. Rev. B 80 (3)*, 035310:7.

Mares, J.J., Siddiki, A., Kindl, D., Hubik, P., & Kristofik, J. (2009). Electrostatic screening and experimental evidence of a topological phase transition in a bulk quantum Hall liquid. *New Journal of Physics 11 (8)*, 083028.

Matthews, J., & Cage, M.E. (2005). Temperature dependence of the Hall and longitudinal resistances in a quantum Hall resistance standard. *J. Res. Natl. Inst. Stand. Technol. 110* 497-500.

Nixon, J.A., Davies, J.H. (1990). Potential fluctuations in heterostructure devices. *Phys. Rev. B 41* 7929-7932.

Oh, J. H., & Gerhardts, R. R. (1997). Self-consistent Thomas-Fermicalculation of potential and current distributions in a to-dimensional Hall bar geometry. *Phys. Rev. B*, *56 (20)*, 13519-13528.

Prange, R. E., & Girvin, S.M. (1987)in *The Quantum Hall Effect* Springer: New York.

Prange, R. (1981) *Phys. Rev. B 23*, 4802.

Ramvall, P., Carlsson, N., Omling, P., Samuelson, L., Seifert, W., Wang, Q., Ishibashi, K., & Aoyagi, Y. (1998). Quantum transport in high mobility modulation doped $Ga_{0.25}In_{0.75}As/InP$ quantum wells. *J. Appl. Phys. 84* 2112-2123.

Richter, C.A., Wheeler, R. G., & Sacks, R. N. (1992). Transitions between edge and bulk channels in the quantum Hall regime. *Surf. Sci. 263* 270.

Ruhe, N., Springborn, J.I., Heyn, C., Wilde, M.A., & Grundler, D. (2006). Simultaneous measurement of the de Haas-van Alphen and the Shubnikov-de Haas effect in a two-dimensional electron system. *Phys. Rev. B 74 (23)* 235326:6.

Sailer, J., Wild, A., Lang, V., Siddiki, A., & Bougeard, D. (2010). *ArXiv e-prints* .

Şakiroğlu, S., & Räsänen, E.,(2010). Colle-Salvetti-type local density functional for the exchange-correlation energy in two dimensions, *Phys. Rev. A*, *82 (1)*, 012505/1-5.

Schweitzer, L., Kramer, B., & MacKinnon, A. (1985). *Z. Physik B 59* 379

Scher, H., & Holstein, T. (1966). High-Frequency Cyclotron Resonance in an Electron-Phonon Gas. *Physical Review* 148 598-631.

Shlimak, I., Ginodman, V., Gerber, A.B., Milner, A., Friedland, K.J., & Paul, D.J. (2005). Manifestation of the Exchange Enhancement of the Valley Splitting in the Quantum Hall Effect. *Europhys. Lett. 69* 997-1002.

Shlimak, I., Friedland, K.-J., Ginodman, V., & Kravchenko, S. (2006). Disorder-induced features of the transverse resistance in a Si-MOSFET in the quantum Hall effect regime. *phys. status solidi (c) 3* 309-312.

Siddiki, A. (2005). *Model Calculations of Current and Density Distributions in Dissipative Hall Bars*. Stuttgart: Ph.D. Thesis.

Siddiki, A., (2007). Self-consistent Coulomb picture of an electron-electron bilayer system,*Phys. Rev. B*, *75 (15)*, 155311/1-15.

Siddiki, A. (2008). The spin-split incompressible edge states within empirical Hartree approximation at intermediately large Hall samples. *Physica E*, *40(5)*, 1124-1126.

Siddiki, A., & Gerhardts, R. R. (2003). Thomas-Fermi-Poisson theory of screening for laterally confined and unconfined two-dimensional electron systems in strong magnetic fields, *Phys. Rev. B*, *68 (12)*, 125315/1-12.

Siddiki, A., & Gerhardts, R. R. (2004). Incompressible strips in dissipative Hall bars as origin of quantized Hall plateaus, *Phys. Rev. B*, *70 (19)*, 195335.

Siddiki, A., & Marquardt, F. (2007). Self-consistent calculation of the electron distribution near a quantum point contact in the integer quantum Hall effect, *Phys. Rev. B*, *75 (4)*, 045325/1-11.

Siddiki, A., & Gerhardts, R.R. (2007). Range-Dependent Disorder Effects On The Plateau-Widths Calculated Within The Screening Theory Of The IQHE. *Int. J. of Mod. Phys. B 21* 1362.

Siddiki, A., & Gerhardts, R.R. (2002). *Nonlinear Thomas-Fermi-Poisson theory of screening for a Hall bar under strong magnetic fields*, in *Proc. 15th Intern. Conf.*

on High Magnetic Fields in Semicond. Phys., edited by A.R. Long, J.H. Davies (Institute of Physics Publishing, Bristol)

Siddiki, A., Horas, J., Moser, J., Wegscheider, W., & Ludwig, S. (2009). Interaction mediated asymmetries of the quantized Hall effect. *Europhysics Letters 88* 17007.

Siddiki, A., Horas, J., Kupidura, D., Wegscheider, W., & Ludwig, S. (2010). Asymmetric nonlinear response of the quantized Hall effect. *New Journal of Physics 12* 113011.

Slevin, K., & Ohtsuki, T. (2009). Critical exponent for the quantum Hall transition. *Phys. Rev. B 80(4)* 041304:4.

Steele, G.A., Ashoori, R.C., Pfeiffer, L.N., & West, K.W. (2005). Imaging Transport Resonances in the Quantum Hall Effect. *Physical Review Letters 95 (13)* 136804:4.

Streda P & Smrcka L 1983 Thermodynamic derivation of the Hall current and the thermopower in quantising magnetic field *J. Phys. C: Solid State Phys. 16* 895û9

Stopa, M., & Aoyagi, Y. (1996). Effect of donor layer ordering on the formation of single mode quantum wires. *Physica B Condensed Matter 227* 61-64.

Suddards, M. E. (2007). Scanning Capacitance Microscopy in the Quantum Hall Regime. *University of Nottingham.*

Suzuki, T., & Ando, T. (1993). *J. Phys. Soc. Jpn. 62* 2986.

Thouless, D.J., Kohmoto, M., Nightingale, M.P., & Nijs, M. den. (1982). Quantized Hall Conductance in a Two-Dimensional Periodic Potential. *Phys. Rev. Lett. 49* 405.-408

Tsui, D. C., Störmer, H. L., & Gossard, A. C. (1982). Two-Dimensional Magneto-transport in the Extreme Quantum Limit. *Phys. Rev. Lett., 48 (22)*, 1559-1562.

Weichselbaum, A., & Ulloa, S.E. (2003). Potential landscapes and induced charges near metallic islands in three dimensions. *Phys. Rev E 68(5)* 056707:5.

Wei, Y.Y., Weis, J., Klitzing, K. v., & Eberl, K. (1997). Single-electron transistor as an electrometer measuring chemical potential variations. *Appl. Phys. Lett. 71* 2514.

Wei, Y.Y., Weis, J., Klitzing, K. v., & Eberl, K. (1998). Single-electron transistor as an electrometer on a two-dimensional electron system. *Physica B 496* 249-251.

Weitz, P., Ahlswede, E., Weis, J., Klitzing, K. v., & Eberl. (2000). Hall-Potential Investigations under Quantum Hall Conditions Using Scanning Force Microscopy. *Physica E*, *6*, 247-250.

APPENDIX A

A.1 Hermite Polynomials

A.1.1 Generating function

The Hermite polynomials Arfken (1995), $H_n(x)$, may be defined by the generating function

$$g(x,t) = e^{-t^2+2tx} = \sum_{n=0}^{\infty} H_n(x)\frac{t^n}{n!} \tag{A.1.1}$$

From the generating function we find that the Hermite polynomials satisfy the recurrence relations

$$H_{n+1}(x) = 2xH_n(x) - 2nH_{n-1}(x) \tag{A.1.2}$$

and

$$H_n^{'}(x) = 2nH_{n-1}(x). \tag{A.1.3}$$

From above two relations follow differential equation for Hermite Polynomials

$$H_n^{''}(x) - 2nH_n^{'}(x) + 2nH_n(x). \tag{A.1.4}$$

The first five Hermite polynomials are

$$H_0(x) = 0 \tag{A.1.5}$$

$$H_1(x) = 2x \tag{A.1.6}$$

$$H_2(x) = 4x^2 - 2 \tag{A.1.7}$$

$$H_3(x) = 8x^3 - 12x \tag{A.1.8}$$

$$H_4(x) = 16x^4 - 48x^2 + 12 \tag{A.1.9}$$

A.1.2   Another formalism

Differentiation of the generating function n times with respect to t and then setting $t = 0$ yields

$$H_n(x) = (-1)^n e^{x^2} \frac{d^n}{dx^n}(e^{-x^2}) \tag{A.1.10}$$

Hermite polynomial $H_n(x)$ in series form is

$$H_n(x) = e^{x^2/2}(x - \frac{d}{dx})e^{-x^2/2} \tag{A.1.11}$$

Another operator representation of Hermite polynomial is

$$H_n(x) = \sum_{s_0}^{[n/2]} (-1)^s (2x)^{n-2s} \frac{n!}{(n-2s)!s!} \qquad (A.1.12)$$

APPENDIX B

B.2   The Fourier Expansion of the Coulomb Potential

$$V(\overrightarrow{q},z) = \int d\overrightarrow{r}\, e^{i\overrightarrow{q}\cdot\overrightarrow{r}} \sum_{j=1}^{N} \frac{e^2/\overline{\kappa}}{\sqrt{(\overrightarrow{r}-\overrightarrow{r_j}+z^2)}} \Big|_{\overrightarrow{q=2D}} \tag{B.2.1}$$

$$\frac{1}{\sqrt{(\overrightarrow{r}-\overrightarrow{r_j}+z^2)}} = \frac{2}{(2\pi)^2} \int \frac{d\overrightarrow{Q}\, e^{iQ(\overrightarrow{r}-\overrightarrow{r_j})+z\widehat{z}}}{Q^2} \tag{B.2.2}$$

$$\frac{2}{(2\pi)^2} \int dQ_z \int \frac{d\overrightarrow{Q}\, e^{iQ(\overrightarrow{r}-\overrightarrow{r_j})}e^{iQ_z}}{Q_H^2+Q_z^2} \tag{B.2.3}$$

$$V(\overrightarrow{q},z) = \sum_{j=1}^{N} e^2/\overline{\kappa} \int Q_K \int dz\, e^{i(\overrightarrow{Q_H}-\overrightarrow{q})\overrightarrow{r}} e^{-iQ_H\overrightarrow{r_j}} \tag{B.2.4}$$

$$\frac{2}{(2\pi)^2} \int dQ_z e^{iQ_z z} \frac{1}{Q_H^2+Q_z^2} \tag{B.2.5}$$

$$= \sum_{j=1}^{N} \frac{e^2}{\overline{\kappa}} \int_0^{\infty} dQ_z \frac{e^{iQ_z z}}{(q^2+Q_z^2)} \tag{B.2.6}$$

$$V(\overrightarrow{q},z) = \frac{2\pi e^2}{\overline{\kappa}} \frac{e^{-|q|z}}{q} NS(\overrightarrow{q}) \frac{\pi e^{-|q|z}}{q} \tag{B.2.7}$$

$$NS(q) = \sum_{j=1}^{N} e^{-i\vec{q}\,\vec{r_j}} \tag{B.2.8}$$

$$V(\vec{q},z) = \frac{2\pi e^2 e^{-|q|z}}{\overline{\kappa}q}(\sum_{j=1}^{N}(e^{-i\vec{q}\vec{r_j}})) \tag{B.2.9}$$

APPENDIX C

C.3   In-plane Charges and Gates

We assume a two-dimensional split-gate structure lies the interface between two semiconductors which occupy the half spaces $z > 0$ and $z < 0$ with translation invariance in the y-direction (Güven, & Gerhardts, 2003). Two semi-infinite metal gates extended at $x < -d$ and $x > d$ with constant potentials V_L and V_R, respectively and the Hall bar is defined along the y-direction on the $x - y$ plane and in the presence of a magnetic field applied along the z-direction. Thus, the charge density is only a function of x and z and has a form $\rho(x)\delta(z)$. The surface charge density $\rho(x)$ given by;

$$\rho(x) = e(n_D - n_{el}(x)), \tag{C.3.1}$$

Here, n_D is positively charged particles and n_{el} is surface densities of electrons. Although the system is symmetric around $x = 0$, we can obtain an asymmetric charge density $\rho(x)$ by applying $V_L - V_R \neq 0$ between the metal gates. The electrostatic potential $V(x,z)$ is obtained by solving 2D Laplace equation

$$\nabla^2_{x,z}V(x,z) = 0, \tag{C.3.2}$$

using the theory of complex functions as follows. The electrostatic potential, first one is that the electrostatic potential should be V_L and V_R, in the regions of the metal gates. Second one is that the inside the Hall bar, the normal derivative of the electrostatic potential should be given by the surface charge density $\rho(x)$.

The boundary conditions are defined,

$$V(x, z = 0) = \begin{cases} V_L & x < -d, \\ V_R & x > d. \end{cases} \tag{C.3.3}$$

The potential $V(x,z)$ depends on the boundary condition resulting from the displacement field of the charge density $\rho(x)$ for $|x| < d$,

$$\kappa_> \frac{\partial V}{\partial z}(x,z=0^+) - \kappa_< \frac{\partial V}{\partial z}(x,z=-0^+) = -4\pi\rho(x), \tag{C.3.4}$$

and $V(x,0) = 0$ for $|x| > d$. Using the conventional theory of analytic functions, one writes $V(x,z)$ as the imaginary part of a holomorphic function $F(\zeta)$ in the complex plane, $V(x,z) = ImF(\zeta)$ and $\zeta = x + iz$.

$$\frac{\partial V(x,z)}{\partial x} = \frac{\partial V}{\partial \zeta} = Im\left(\frac{dF}{d\zeta}\right) \tag{C.3.5}$$

$$\frac{\partial V}{\partial z} = i\frac{\partial V}{\partial \zeta} = Im\left[i\frac{\partial F}{\partial \zeta}\right]$$

$$= Im\left[i\left(Re\left(\frac{\partial F}{\partial \zeta}\right) + Im\left(\frac{\partial F}{\partial \zeta}\right)\right)\right]$$

$$\frac{\partial V}{\partial z} = Re\left(\frac{\partial F}{\partial \zeta}\right) \tag{C.3.6}$$

where $F(\zeta)$ satisfies the following boundary conditions;

$$Re\frac{dF}{d\zeta}\Big|_{\zeta=x+i0^+} = r(x) \qquad |x| < d, \tag{C.3.7}$$

$$Im\frac{dF}{d\zeta}\Big|_{\zeta=x+i0^-} = 0 \qquad |x| > d, \tag{C.3.8}$$

and $r(x)$ is defined as in the Equation C.3.4.

$$\kappa_> \frac{\partial V}{\partial z}(x,z) + \kappa_< \frac{\partial V}{\partial z}(x,z) = -4\pi\rho(x),$$

$$(\kappa_> + \kappa_<)\frac{\partial V}{\partial z}(x,z) = -4\pi\rho(x),$$

$$\frac{\partial V}{\partial z}(x,z) = -\frac{4\pi}{\kappa_> + \kappa_<}\rho(x). \tag{C.3.9}$$

Here,

$$\bar{\kappa} = \frac{\kappa_> + \kappa_<}{2} \Rightarrow \frac{\partial V_2}{\partial_z}(x,z) = -\frac{2\pi}{\bar{\kappa}}\rho(x) = r(x). \tag{C.3.10}$$

and $\bar{\kappa}$ is the average dielectric constant. The above boundary conditions define the discontinuity of the auxiliary function which has an identical solution,

$$h(\zeta) = i\sqrt{d^2 - \zeta^2}\frac{\partial F}{\partial \zeta}, \tag{C.3.11}$$

along the real axis and gives rise to

$$Imh(x+i0^+) = \begin{cases} r(x)\sqrt{d^2 - x^2} & for & |x| < d, \\ 0 & for & |x| > d, \end{cases} \tag{C.3.12}$$

where $\sqrt{d^2 - \zeta^2}$ is holomorphic, except for the branch cut ($|x| > d$). In all of space, this function can be obtained using the Schwartz integral as,

$$h(\zeta) = \frac{1}{\pi}\int_{-\infty}^{\infty} dx \frac{Imh(x+i0^+)}{x-\zeta} + c = \frac{1}{\pi}\int_{-d}^{d} dx \frac{r(x)\sqrt{d^2 - x^2}}{x-\zeta} + c, \tag{C.3.13}$$

with real constant of integration c. Equation C.3.11 and Equation C.3.13 are equal to each other. The solution of $V_2(x)$ is obtained;

$$i\sqrt{d^2 - \zeta^2}(\frac{\partial F}{\partial \zeta}) = \frac{1}{\pi}\int_{-d}^{d} dxr(x)\frac{\sqrt{d^2 - x^2}}{x-\zeta} + c, \tag{C.3.14}$$

and can be written as,

$$F = -i\left\{\frac{1}{\pi}\int_{-d}^{d} dx'r(x')K(x,x') + \left(c\int d\zeta \frac{1}{\sqrt{d^2 - \zeta^2}} + c_1\right)\right\}. \tag{C.3.15}$$

Thus, the electrostatic potential can be written in the form,

$$V(x) = V_H(x) + V_G(x) + V_D(x), \tag{C.3.16}$$

$$V_H(x,z) = Im(F(\zeta)) \qquad \Rightarrow \qquad V_H(x) = -\frac{1}{\pi}\int\limits_{-d}^{d} dx' r(x') K(x,x')$$

<div align="center">(C.3.17)</div>

$$K(x,x') = ln\left|\frac{\sqrt{(d^2 - x^2)(d^2 - x'^2)} + d^2 - xx'}{(x - x')d}\right|.$$

The Hartree potential $V_H(x)$ is uniquely determined by Equation C.3.17. Where the kernel $K(x,x')$ solves Poisson's equation under the given boundary conditions. The donor and the Hartree potentials vanish if $r(x) = 0$, thus we obtain the gate potential as;

$$V = c\int d\zeta \frac{1}{\sqrt{d^2 - \zeta^2}} + c_1 = V_G, \qquad (C.3.18)$$

$$\int d\zeta \frac{1}{\sqrt{d^2 - \zeta^2}} = sin^{-1}(x/d) \quad \Rightarrow \quad V_G = c \cdot sin^{-1}(x/d) + c_1. \qquad (C.3.19)$$

According to the boundary conditions, one determines the real constants to be,

$$V_L = -c\frac{\pi}{2} + c_1 \qquad and \qquad V_R = c\frac{\pi}{2} + c_2, \qquad (C.3.20)$$

with, $c_1 = \frac{1}{2}(V_L + V_R)$ and $c_2 = \frac{1}{\pi}(V_R - V_L)$. Therefore, the gate potential and the energy are determined by these constants;

$$V_G(x) = \frac{1}{\pi}(V_R - V_L)sin^{-1}(\frac{x}{d}) + \frac{1}{2}(V_L + V_R). \qquad (C.3.21)$$

Assuming $V_G = 0$,

$$V_D + V_H = -\frac{1}{\pi}\int\limits_{-d}^{d} dx' \left(\frac{2\pi e^2}{\bar{\kappa}}\right)(n_D - n_{el}(x'))K(x,x'), \qquad (C.3.22)$$

Donor potential is obtained as,

$$
\begin{aligned}
V_D &= -\frac{1}{\pi} \int_{-d}^{d} dx' \left(\frac{2\pi e^2 n_D}{\bar{\kappa}} K(x,x') = -\frac{2e^2}{\bar{\kappa}} n_D \int_{-d}^{d} dx' K(x,x'), \right. \\
&= -\frac{2\pi e^2 n_D}{\bar{\kappa}} \left(d\sqrt{1 - \left(\frac{x}{d}\right)^2} \right) = -E_0 \sqrt{1 - \left(\frac{x}{d}\right)^2}.
\end{aligned} \qquad \text{(C.3.23)}
$$

where E_0 is the pinch-off energy and defined as $(2\pi e^2 n_D d)/(\bar{\kappa}) = E_0$. This potential results from the positive background charges and has an elliptic shape with the minimum value at $x = 0$.

ABBREVIATIONS and SYMBOLS

QHE	Quantum Hall Effect
IQHE	Integer Quantum Hall Effect
2DEG	Two-dimensional electron gas
LL(s)	Landau level(s)
IS(s)	Incompressible strip(s)
DOS	Density of states
LDOS	Local Density of states
TFA	Thomas Fermi Approximation
3D	Three Dimensional
QHP	Quantum Hall Plateu
$\mathbf{E}$	Electric Field
m_0	Electron mass
m^*	Effective electron mass
m_p	Modulation period
μ^*	Electrochemical potential
V_{bg}	Background potential
V_H	Hall potential
V_{imp}	Impurity potential
V_d	Drift Velocity
ν	Filling Factor
$a_B^* = \bar{\kappa}\hbar^2/(me^2)$	Effective Bohr radius
$a_0 = a_B^*/2$	Screening length
$a_k =$	The width of the incompressible stripes
E_F	Fermi energy
$E_0 = 2\pi e^2 n_0 d/\bar{\kappa}$	Pinch-off energy
E_N	Energy of the Nth Landau level
N_I	The number density of the impurities

Γ_N	Width of the Landau level
$\ell_B = \sqrt{\hbar/m\omega_c}$	Magnetic length
$\omega_c = eB/mc$	Cyclotron frequency
τ	The momentum relaxation time
γ_I	the impurity strength